Università degli Studi di Padova

Dipartimento di Fisica e Astronomia

Corso di Laurea Magistrale in Fisica

Localization transitions in coupled Aubry-André chains

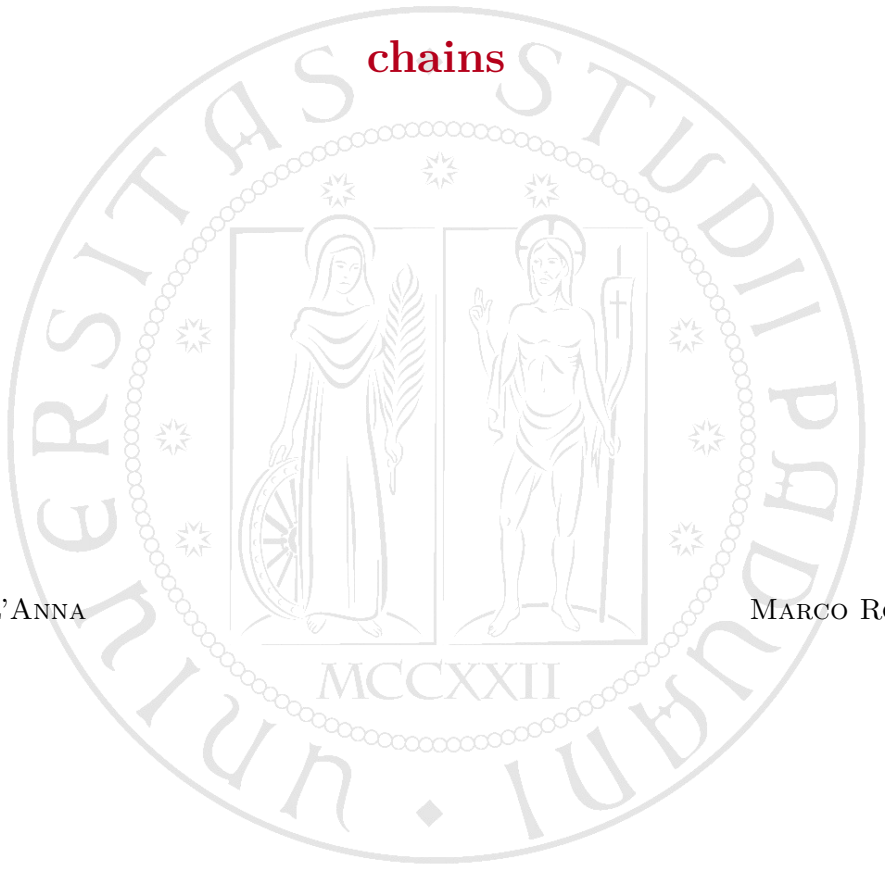

Relatore
Luca Dell'Anna

Laureando
Marco Rossignolo

Contents

Introduction

Since 1958, the year in which Anderson localization was discovered, the problem of electron localization in low dimensional quantum systems has attracted a lot of interest in the scientific community. Anderson localization predicts that the electronic wavefunctions may become localized in imperfect crystals and leads to a disorder-induced metal-insulator transition, caused by the *quantum interference* between multiple scattering of an electron with random impurities and defects.
The localization effect discovered by Anderson, is a *single-particle* phenomenon. Let us consider a free particle of mass m and energy E, in a d-dimensional quenched potential $V(\mathbf{r})$. Its wavefunction $\psi(\mathbf{r})$ satisfies the following Schrödinger equation

$$-\frac{\hbar^2\nabla^2}{2m}\psi(\mathbf{r}) + V(\mathbf{r})\psi(\mathbf{r}) = E\psi(\mathbf{r})\,.$$

In free space, $\psi(\mathbf{r})$ is an extended plane wave, but it can be shown rigorously that, in the presence of disorder, any solution with arbitrary E is exponentially localized in one dimension, namely $\ln(|\psi(z)|) \sim |z|/L_{loc}$, with localization length $L_{loc} \propto l_b$, where l_b is the Boltzmann transport mean-free path.
Even though L_{loc} often increases with E, it is striking that interference effects of multiple scattered waves are strong enough to profoundly affect $\psi(z)$ even for very high energies.
In one dimension, even for arbitrarily weak disorder, all the one-electron states are exponentially localized, for any energy of the system. In other words the system does not present a mobility edge, that is the energy eigenvalue separating localized (insulating) states from the extended (conducting) ones. On the contrary positional correlations of defects can lead to some extend states.
In two dimensions, the situation is similar, but interference effects are weaker and $L_{loc} \propto l_b e^{\pi k l_b/2}$, where $k = \sqrt{2mE}/\hbar$ is the particle wave vector in free space. Hence L_{loc} explodes exponentially for $k > 1/l_b$, inducing a crossover from extended to localized states in finite-size system.
The situation is completely different in three dimensions, where the *Anderson transition* occurs at the so-called *mobility edge*: although low-energy states with $k < k_{mob}$ are exponentially localized, those with $k > k_{mob}$ are extended. The presence of mobility edge can be determined by the *Ioffe-Regel criterion* which basically states that localization requires that the phase accumulated between two successive deflecting scattering processes is less than 2π. In other words, the De Broglie wavelength must exceed the memory of the initial particle direction, thus yielding $k_{mob} \sim 1/l_b$.
Contrary to the one- and two-dimensional cases, in three dimensions the localization of the wavefunctions occurs for a large enough strength of disorder.

However, in atomic crystals important deviations from the Anderson model always occur, because of thermally excited phonons and electron–electron interactions. Realizing that Anderson localization is a wave phenomenon relying on interference, these concepts were extended to optics. A similar phenomenon of the interference of electrons with defects is the multiple scattering of electromagnetic waves but with the simplification that photons do not interact with each other.
In 1997 Diederik et al [1] reported direct experimental evidence of Anderson localization of light in optical experiments. The main difficulty for its detection was the realization of strong enough scattering. This problem was exceeded using semiconductor powders.
This result makes transport of photons in disordered materials an ideal system where to study Anderson localization.
The propagation of light is generally described by a normal diffusion process where the Ohm's law holds with the consequence that the transmission, or conductance, decreases linearly with the system length.
This trend is not fulfilled once the the Anderson localization occurs, making manifest the transition from delocalized to localized states. This change can be observed in the transmission properties of the system: in the localized state the transmission coefficient decreases exponentially instead of linearly with the thickness of the sample.
In 2007-2008, the works [2], [3] reported the experimental observation of Anderson localization in a perturbed period potential observed by the transversed localization of light caused by random fluctuations on a two-dimensional photonic-lattice.

In 2008 Hefei et al. [4] reported the *first observation* of sound localization in a random three dimensional elastic network. They studied the time-dependent transmission below the mobility edge, and observed transverse localization in three dimensions, which has never been observed previously in any wave.
The work [5] paid the attention to the remarkable aspect of multifractality of wavefunctions at Anderson transition. The experimental data was based on the excitation of elastic waves in an open 3D disordered medium. All results was compared with the corresponding analysis of diffusive wave functions in the same network, showing a very clear difference between localized and diffusive regimes.

Anderson Localization in matter waves was observed in 2008 by Billy's [6] and Roati's [7] experiments.
In the first work the authors observed directly exponential localization of a Bose-Einstein condensate released into a one-dimensional waveguide in the presence of a controlled disorder created by *laser speckle*, light patterns resulting from the reflection of coherent light on rough surfaces.
They operated in a regime of weak disorder and at low atomic density so that interactions can be neglected.
Letting the atomic density evolve in time, the disorder can stop the expansion leading to the formation of a stationary, exponentially localized wavefunctions, a direct signature of Anderson localization. In particular, through the analysis of the power spectrum of the one-dimensional speckle potential, the localization occurs only when the De Broglie wavelengths of the atoms in the expanding condensate are greater than an effective mobility edge. Meanwhile, in the opposite case, the density profiles decay algebrically.

The experiment by Roati and coworkers [7] was performed with a one-dimensional quasi-periodic lattice. This system presents a transition between extended and exponentially localized states, as Anderson localization in higher dimensions. The localization effect can be clearly shown through the investigations of the transport properties and spatial and momentum distributions. This experiment was possible thanks to the combination of ultracold atoms and optical potentials. This setup offers a platform for the study of disorder-related phenomena where most of the relevant parameters, including those governing interactions, can be controlled.
The investigation of physics disorder was made possible by the introduction of a quasi-periodic optical lattice. They studied localization in a one-dimensional lattice perturbed by a second, weaker lattice with an incommensurate wavelength, which allows for an experimental realization of the so-called Aubry-André model.
These two experiments are complementary rather than similar [8]. In [6], a weakly interacting BEC is created in a trap, which is abruptly switched off at time t = 0. Then, the condensate expands in a guide in presence of disorder created with optical speckle.
This physics is described by the Gross-Pitaevskii equation:

$$i\hbar\frac{\partial\psi}{\partial t} = -\frac{\hbar^2\nabla^2}{2m}\psi + V(\mathbf{r})\psi + g\left|\psi\right|^2\psi$$

which corresponds to the equations of motion of the Hamiltonian:

$$\hat{\mathcal{H}} = \int d\mathbf{r}\hat{\psi}^\dagger(\mathbf{r})\left[-\frac{\hbar^2\nabla^2}{2m} + V(\mathbf{r})\right]\hat{\psi}(\mathbf{r}) + \frac{g}{2}\int d\mathbf{r}\hat{\psi}^\dagger(\mathbf{r})\hat{\psi}^\dagger(\mathbf{r})\hat{\psi}(\mathbf{r})\hat{\psi}(\mathbf{r})$$

in the mean-field regime.
The dynamics of the BEC can be understood in a two-stage scheme. In the first stage, it is dominated by interactions and the BEC expands, creating a coherent wavefunction with a stationary momentum distribution, $D(k) \propto 1-(k\xi)^2$, where $\xi = \hbar/\sqrt{4m\mu}$ is the initial healing length, which measures the initial interaction strength, and μ is the initial chemical potential of the BEC.
In the second stage, once the expansion has strongly lowered the atomic density $|\psi(z)|^2$, the interaction term vanishes and we are left with a superposition of (almost) non-interaction term ψ_k; the population of each is $D(k)$.
Then each ψ_k eventually becomes localized through the scattering with the disordered potential, so that $\ln(|\psi_k(z)|) \sim |z|/L_{loc}(k)$, and the total BEC density reduces to $n_{BEC}(z) \backsimeq \int dk D(k)\left\langle|\psi_k(z)|^2\right\rangle$.
Direct imaging of the localized matter wave reveals exponentially decaying tails, with a localization length equal to that of a non interacting particle with momentum $k = 1/\xi$. Hence, this experiment corresponds to a transport scheme, which probes Anderson localization of non-interacting particles with a wavevector controlled by the initial interaction, through the healing length ξ.
In contrast the experiment [7] uses a static scheme. The interaction are switched off already in the trap using *Feshbach resonances* [9],so that the gas is created in a superposition of a few low-energy single-particle eigenstates. They are subsequently imaged in situ, revealing exponentially decaying tails.

Strongly motivated by the work by Roati et al. [7] and the experimental feasibility of realizing several copies of the Aubry-André system, we investigate the localization transitions for coupled-chains in a quasi-disordered environment. We use the tight binding approximation in which the electrons are assumed to occupy the standard orbital atoms and the overlap between atomic function on neighboring sites is small.
In the first chapter we review the Aubry-André model and discuss the single particle localization properties supported by numerical calculations using the inverse participation ratio (IPR) function and the Shannon entropy. In the second chapter we characterize the localization transitions with the fractal dimension improving the Economou results. The third chapter is devoted to the effects of next-nearest neighbor in a Aubry-Andrè chain and the rise of mobility-edge.
In the fourth and five chapters we study the localization transition in two weakly coupled chain with different geometry. Using an exact canonical transformation in the cases that present symmetry and a perturbation approach in the others, we have decoupled these systems into two independent Aubry-André chains. Finally, in the last chapter, we summarize our results.

Chapter 1

Aubry-André model

The Aubry-André model [10], already in one-dimension, give rise to a non trivial behavior. It displays a localization transition from delocalized to localized states. A comparison between the Anderson model and the Aubry-André model on the basis of phase-space methods has recently allowed to gain additional insight into the mechanism of the delocalization-localization in these models [11].
In the following, we give a discussion of this model accompanied by numerical results.
The almost Mathieu operator [12]

$$\mathcal{H} = \sum_n \left(|n\rangle \langle n+1| + |n+1\rangle \langle n| \right) + \lambda \sum_n \cos(2\pi\tau n) |n\rangle \langle n| \tag{1.1}$$

considered within the Aubry-André model can be viewed as describing the motion of a particle on a one dimensional lattice where $|n\rangle$ is a Wannier state at lattice site n.
The Hamiltonian $\mathcal{H}$ depends on two parameters: the potential strength λ, taken in units of hopping matrix element and the period of the potential determined by τ.
For $\lambda = 2$, it was demonstrated by Harper [13] that this Hamiltonian describes an electron on a square lattice in a perpendicular magnetic field, a situation first discussed by Peierls [14].
In this case, the parameter $\tau = \Phi/\Phi_0$ corresponds to the flux Φ per plaquettes in units of the flux quantum $\Phi_0 = h/e$. It was found by Hofstadter [15] that the character of the energy spectrum crucially depends on the value of τ. Whereas irrational values of τ lead to a self-similar spectrum, this is not the case for rational τ. The peculiarity of a self-similar energy spectrum suggests to study the Hamiltonian as a function of the potential strength λ while fixing τ at an irrational value. Then, the potential is incommensurate with the underlying lattice and one obtains a quasiperiodic potential.
Following Aubry and André [10], one may expect a phase transition from extended to localized states as λ is increased beyond a critical value $\lambda_c = 2$. However, later it was proved that somewhat stronger requirements need to be imposed on τ. A necessary and sufficient condition for a phase transition to occur in the Aubry–André model is that τ is a Diophantine number [12]. In the following, we will use the inverse of the golden mean, $\tau = (\sqrt{5}-1)/2$, which is Diophantine and a common choice in studies of the Aubry–André model.
The inverse of the golden mean is a convenient choice [16] because the convergents of its continued fraction representation are given by ratios of successive Fibonacci numbers defined by the recursion relation $F_{n+1} = F_n + F_{n-1}$ with $F_0 = 0$ and $F_1 = 1$.
Therefore, if the system size is chosen as a Fibonacci number F_i , the period τ can be

approximated by F_{i-1}/F_i, which yields the inverse of the golden mean in the limit of large system sizes.
Both, the Hamiltonian and its finite size approximations just discussed, possess a potential which is symmetric with respect to the site $n = 0$. Therefore, energy eigenstates may always be chosen as symmetric or antisymmetric. This not only presents conceptual but also technical advantages because it reduces the Hamiltonian to tridiagonal form even in the presence of periodic boundary conditions [17]. Since in this way much larger system sizes become accessible, we will always consider states of definite symmetry. It was checked that even for rather small system sizes the results do not change if the states of the other symmetry class are taken into account as well.
It defines the state:

$$|k\rangle := \frac{1}{\sqrt{L}} \sum_n e^{i2\pi k\tau n} |n\rangle$$

The reverse transformation is obtained by multiplying both side for $e^{-i2\pi k\tau m}$ and sum over k:

$$\begin{aligned} \sum_k e^{-i2\pi k\tau m} |k\rangle &= \sum_n \sum_k \frac{1}{\sqrt{L}} e^{i2\pi k\tau(n-m)} |n\rangle \\ &= \frac{1}{\sqrt{L}} \sum_n \delta_{n,m} |n\rangle = \sqrt{L} |m\rangle \end{aligned}$$

So :

$$|n\rangle = \frac{1}{\sqrt{L}} \sum_k e^{-i2\pi k\tau n} |k\rangle$$

In the same way it gets:

$$|n\rangle = \frac{1}{\sqrt{L}} \sum_k e^{-i2\pi k\tau n} e^{-i2\pi\tau n} |k+1\rangle$$

Substituting this two result in the Hamiltonian 1.1:

$$\begin{aligned} \mathcal{H} &= \sum_n \sum_k \sum_{k'} \frac{1}{L} e^{-i2\pi k\tau n} e^{i2\pi k'\tau(n+1)} |k\rangle \langle k'| + \frac{1}{L} e^{-i2\pi k\tau(n+1)} e^{i2\pi k'\tau n} |k\rangle \langle k'| \\ &+ \frac{\lambda}{2} \frac{1}{L} \sum_n \sum_k \sum_{k'} \left(e^{i2\pi\tau n} + e^{-i2\pi\tau n} \right) e^{-i2\pi k\tau n} e^{i2\pi k'\tau n} |k\rangle \langle k'| \\ &= \frac{\lambda}{2} \left[\frac{4}{\lambda} \sum_k \cos(2\pi\tau k) |k\rangle \langle k| + \sum_k \left(|k\rangle \langle k+1| + |k+1\rangle \langle k| \right) \right] \end{aligned}$$

The eigenstates of the momentum operator have eigenvalues:

$$\tilde{k} = k\tau$$

In fact the action of momentum operator on its eigenstate is defined by:

$$\begin{aligned}
-i\frac{\partial|k\rangle}{\partial n} &= -i\frac{1}{\sqrt{L}}\partial_n \sum_m e^{i2\pi\tau km}|m\rangle \\
&= -i\frac{1}{\sqrt{L}}\partial_n \sum_m \sum_{k'} e^{i2\pi\tau km}|k'\rangle\langle k'||m\rangle \\
&= -i\frac{1}{\sqrt{L}}\partial_n \sum_m \sum_{k'} e^{i2\pi\tau(k-k')m}|k'\rangle \\
&= \frac{1}{\sqrt{L}} \sum_m \sum_{k'} 2\pi\tau(k-k')e^{i2\pi\tau(k-k')m}|k'\rangle \\
&= \frac{1}{\sqrt{L}} \sum_m \sum_{k'} 2\pi\tau(k-k')e^{i2\pi\tau km}|k'\rangle\langle k'||m\rangle \\
&= \frac{1}{\sqrt{L}} \sum_m 2\pi\tau k e^{i2\pi\tau km}|m\rangle \\
&= 2\pi\tau k|k\rangle
\end{aligned}$$

where the term $\sum_{k'} k'|k'\rangle\langle k'|$ is null for symmetry. The Hamiltonian in real space is thus mapped onto a Hamiltonian of the same form in a permuted momentum space with the original potential strength λ replaced by $4/\lambda$.
The difference between figures real and momenta space is therefore due to the reshuffling of momenta values according to $k = \tilde{k}F_{i-1} \mod F_i$ [11]. Of particular importance is the self-dual point $\lambda = 2$ where the localization transition occurs.

1.1 Model and Method

Within the framework of the tight-binding approximation, the Hamiltonian operator can be written as:

$$\mathcal{H} = \sum_{<n,m>}^{L} \hat{b}_n^\dagger \hat{b}_m + \lambda \sum_n \cos(2\pi\tau n)\hat{b}_n^\dagger \hat{b}_n$$

where $\hat{b}_n^\dagger$ and $\hat{b}_n$ are creation and annihilation operators at lattice site n respectively, L is system size, λ is the potential strength in unit of the hopping coefficient and $\tau = \frac{\sqrt{5}+1}{2}$ is the golden ratio. The Schroedinger equation $\mathcal{H}|\psi\rangle = E|\psi\rangle$ in the site representation can be expressed as:

$$\mathcal{H}_n\psi_n = E\,\mathbb{I}\,\psi_n$$

where $\mathbb{I}$ is the $L \times L$ identity matrix, $\mathcal{H}_n$ is the Hamiltonian matrix of the nth layer

$$\mathcal{H}_n = \begin{bmatrix}
\epsilon_1 & 1 & 0 & \dots & 0 \\
1 & \epsilon_2 & 1 & \ddots & \vdots \\
0 & 1 & \epsilon_3 & \ddots & 0 \\
\vdots & \ddots & \ddots & \ddots & 1 \\
0 & \dots & 0 & 1 & \epsilon_n
\end{bmatrix}$$

and Ψ_n is the amplitude of the wavefuntion at lattice site n.
We note that for $\psi_n \mapsto e^{in\pi}\psi'_n$ the eigenvalue equation

$$t\left(\psi_{n-1} + \psi_{n+1}\right) + \epsilon_n \psi_n = E\psi_n$$

becomes:

$$-t\left(\psi'_{n-1} + \psi'_{n+1}\right) + \epsilon_n \psi'_n = E\psi'_n$$

Due to the fact that the density $|\psi_n|^2$ doesn't change in this transformation, the eigenvalues equation is invariant for $t \mapsto -t$.

1.2 Numerical Calculations

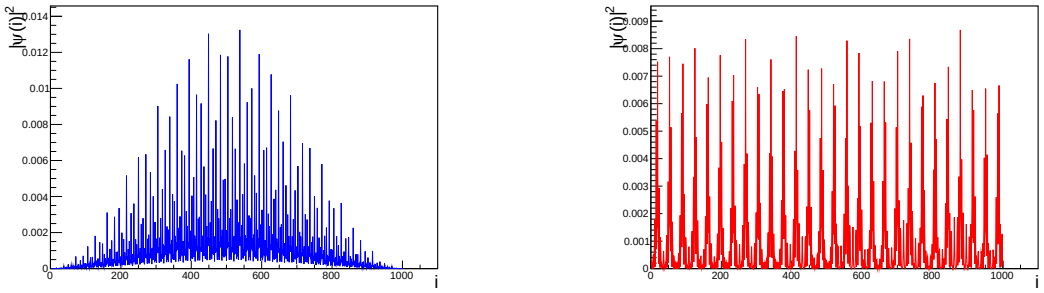

Figure 1.1: Square of the wavefunction versus lattice site i for $\lambda = 1.75$, E_{gs} in blue line (left side) and $E \simeq 0$ in red line (right side)

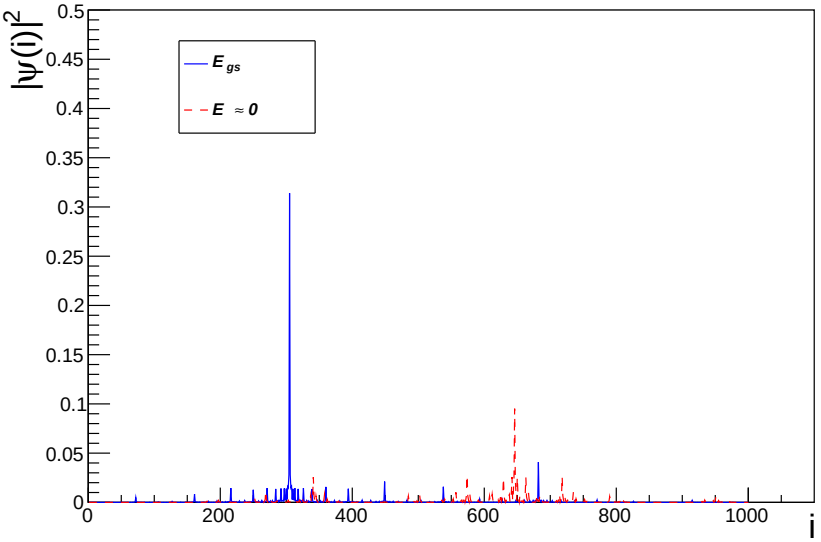

Figure 1.2: Square of the wavefunction versus lattice site i for $\lambda = 2$, E_{gs} in blue continue line and $E \simeq 0$ in red dashed line

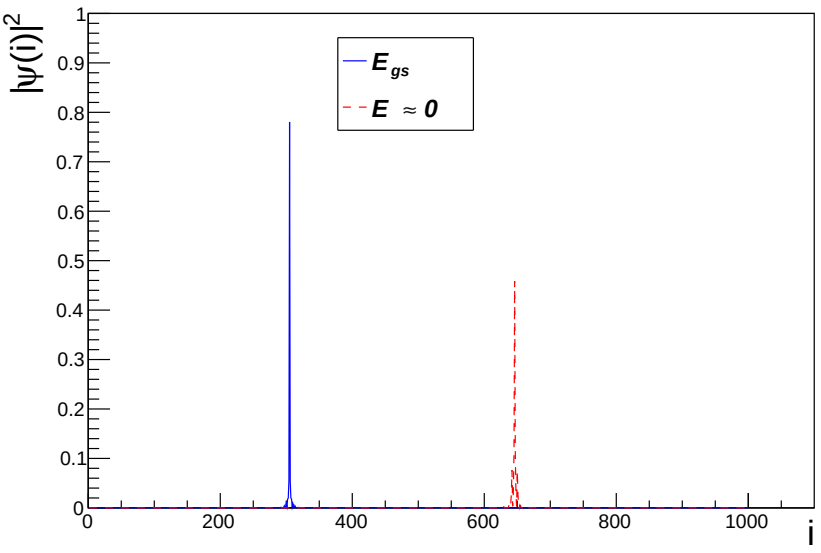

Figure 1.3: Square of the wavefunction versus lattice site i for $\lambda = 2.25$, E_{gs} in blue continue line and $E \simeq 0$ in red dashed line

To attain a clearer picture of the duality of the Aubry–André model, we present the IPR-function [18] in real and momentum spaces, respectively, as a function of the potential strength λ (figure 1.6).
The IPR-function defined by:

$$IPR(q) = \frac{\sum_i |\psi_i|^{2q}}{\sum_i |\psi_i|^2}$$

with $q = 2$.
This function measures the degree of localization of a particle in a certain lattice. For extremely delocalized states the wavefunction is equally distributed and can be approximated as $\psi_i \simeq \frac{1}{L}$, where L is the size of the system. In this limit we have $IPR(2) = \frac{1}{L}$. In the opposite case, when the states are extremely localized, the wavefuntion assumes a non null value only in a determined site l. So we have $\psi_i \simeq \delta_{l,n}$ and $IPR(2) = 1$. In this picture it can be seen the dual point in $\lambda = 2$.
A same way to characterize the localization transition is with Shannon entropy:

$$S = -\sum_i |\psi_i|^2 \ln(|\psi_i|^2)$$

In order to find the critic parameter λ_c, we have calculate numerically the maximum value of IPR's derivate in figure 1.4 and equivalently the minimum value of Shannon entropy's derivate in figure 1.5.
We find that for $\lambda < 2$ all states are localized meanwhile for $\lambda > 2$ all states are delocalized.

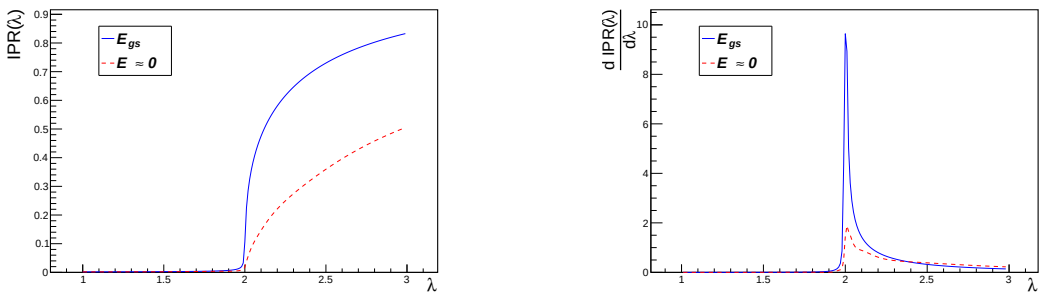

Figure 1.4: IPR-function and its derivate versus the potential strength λ. We plot E_{gs} in blue continue line and $E \simeq 0$ in red dashed line

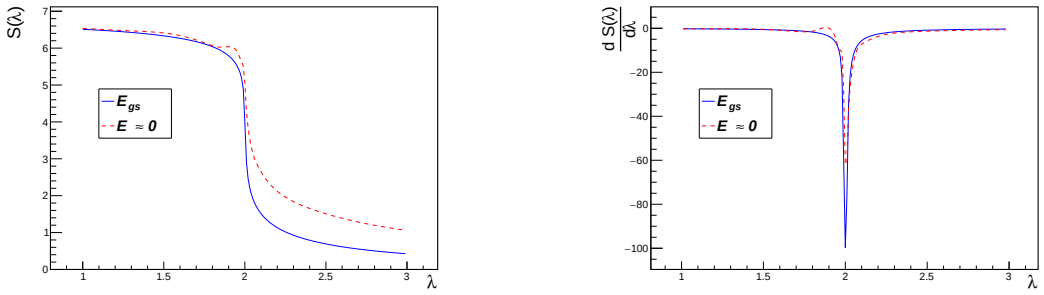

Figure 1.5: Shannon Entropy and its derivate versus the potential strength λ. We plot E_{gs} in blue continue line and $E \simeq 0$ in red dashed line

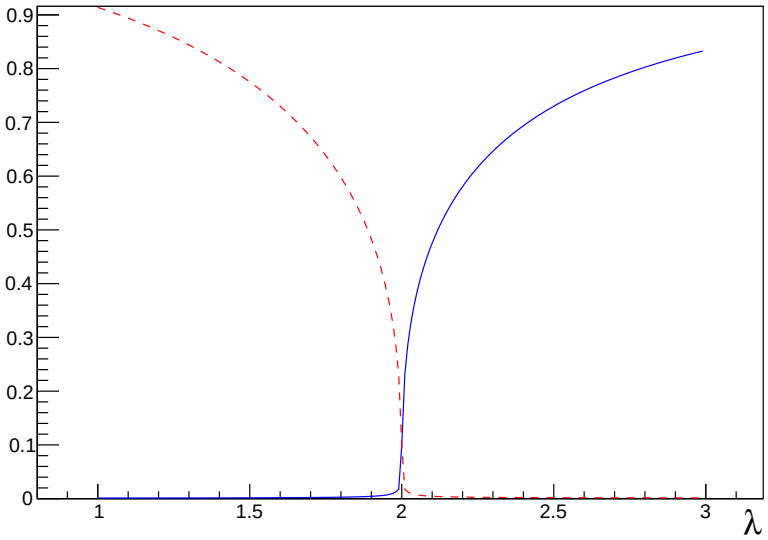

Figure 1.6: IPR in real (blue continue line) and momentum (red dashed line) space

Chapter 2

Fractal dimension

In order to explain the problem of fractal dimension and the presence of localized or delocalized states, we begin this chapter with the mapping of the Hofstader's 2D Hamiltonian into a Aubry-André model in the magnetic field limit of $B \to 0$ [19].
In this perspective we study the eigenstates of 2D Hofstader's Hamiltonian to characterize the localization transition of Aubry-André model.

2.1 Hofstader's model and Aubry-André model

Let's start from tight-binding Hamiltonian:

$$\mathcal{H} = T_x + T_y + h.c.$$

where T_x and T_y are the covariant translation operators by one lattice-constant in the $\hat{\mathbf{x}}$- and $\hat{\mathbf{y}}$- directions, which, when a magnetic field applied, take the covariant form:

$$\begin{cases} T_x = \sum_{m,n} \hat{c}^\dagger_{m+1,n} \hat{c}_{m,n} e^{i\theta^x_{m,n}} \\ T_y = \sum_{m,n} \hat{c}^\dagger_{m,n+1} \hat{c}_{m,n} e^{i\theta^y_{m,n}} \end{cases}$$

Since the Hamiltonian contains only nearest-neighbor terms, the phase factors can be consistently chosen as the integral of the external vector potential over the bond linking the nearest-neighbor, as it is defined in *Peierel*'s substitution:

$$\begin{cases} \theta^x_{m,n} = \frac{e}{\hbar} \int_m^{m+1} \mathbf{A} \cdot d\mathbf{x} \\ \theta^y_{m,n} = \frac{e}{\hbar} \int_n^{n+1} \mathbf{A} \cdot d\mathbf{y} \end{cases}$$

We introduce the lattice derivates:

$$\begin{cases} \Delta_x f_{m,n} = f_{m+1,n} - f_{m,n} \\ \Delta_y f_{m,n} = f_{m,n+1} - f_{m,n} \end{cases}$$

The lattice curl of the phase factors is related to the flux per plaquette $\phi_{m,n}$.

$$\nabla \times \theta_{m,n} = \begin{bmatrix} \Delta_x \\ \Delta_y \\ \Delta_z \end{bmatrix} \times \begin{bmatrix} \theta^x_{m,n} \\ \theta^y_{m,n} \\ 0 \end{bmatrix} = \begin{bmatrix} 0 \\ 0 \\ \Delta_x \theta^y_{m,n} - \Delta_y \theta^x_{m,n} \end{bmatrix}$$

So, using the expression for lattice derivates, we obtain:

$$\nabla \times \theta_{m,n} = (\theta^y_{m+1,n} - \theta^y_{m,n} - \theta^x_{m,n+1} + \theta^x_{m,n})\hat{\mathbf{z}} \qquad = \left[\frac{e}{\hbar}\int_{\text{unit cell}} \mathbf{A}\cdot d\mathbf{l}\right]\hat{\mathbf{z}} = 2\pi\phi_{m,n}\hat{\mathbf{z}}$$

where $\phi_{m,n}$ is the number of flux quanta in units of h/e.
Lattice Hamiltonian has $U(1)$ symmetry: $c_i \mapsto U_i c_i$, $e^{i\theta_{i,j}} \mapsto U_i e^{i\theta_{i,j}} U_j^{-1} = e^{i\theta_{i,j}}$ if and only if $|U_i| = 1\ \forall j \in (m,n)$.
In the weak field limit, $\phi \to 0$, it gives the Landau level structure.
The covariant translation operators do not commute. We define the eigenfunction $|\psi_{m,n}\rangle = \hat{c}^\dagger_{m,n}|0\rangle$ and we make:

$$\begin{aligned}
T_x T_y |\psi_{i,j}\rangle &= T_x T_y \hat{c}^\dagger_{i,j}|0\rangle = T_x \sum_{m,n} \hat{c}^\dagger_{m,n+1}\hat{c}_{m,n} e^{i\theta^y_{m,n}} \hat{c}^\dagger_{i,j}|0\rangle \\
&= T_x \sum_{m,n} \hat{c}^\dagger_{m,n+1} e^{i\theta^y_{m,n}} \left(\delta_{m,i}\delta_{n,j} - \hat{c}^\dagger_{i,j}\hat{c}_{m,n}\right)|0\rangle = T_x e^{i\theta^y_{i,j}} \hat{c}^\dagger_{i,j+1}|0\rangle \\
&= \sum_{m,n} \hat{c}^\dagger_{m+1,n}\hat{c}_{m,n} e^{i\theta^x_{m,n}} e^{i\theta^y_{i,j}} \hat{c}^\dagger_{i,j+1}|0\rangle \\
&= \sum_{m,n} e^{i\theta^y_{i,j}} e^{i\theta^x_{m,n}} \hat{c}^\dagger_{m+1,n}\left(\delta_{m,i}\delta_{n,j+1} - \hat{c}^\dagger_{i,j+1}\hat{c}_{m,n}\right)|0\rangle \\
&= e^{i\left(\theta^y_{i,j} + \theta^x_{i,j+1}\right)} \hat{c}^\dagger_{i+1,j+1}|0\rangle
\end{aligned} \tag{2.1}$$

In the same way:

$$\begin{aligned}
T_y T_x |\psi_{i,j}\rangle &= T_y T_x \hat{c}^\dagger_{i,j}|0\rangle = T_y \sum_{m,n} \hat{c}^\dagger_{m+1,n}\hat{c}_{m,n} e^{i\theta^x_{m,n}} \hat{c}^\dagger_{i,j}|0\rangle \\
&= T_x \sum_{m,n} \hat{c}^\dagger_{m+1,n} e^{i\theta^x_{m,n}} \left(\delta_{m,i}\delta_{n,j} - \hat{c}^\dagger_{i,j}\hat{c}_{m,n}\right)|0\rangle \\
&= \sum_{m,n} \hat{c}^\dagger_{m,n+1}\hat{c}_{m,n} e^{i\theta^y_{m,n}} e^{i\theta^x_{i,j}} \hat{c}^\dagger_{i+1,j}|0\rangle \\
&= e^{i\left(\theta^y_{i+1,j} + \theta^x_{i,j}\right)} \hat{c}^\dagger_{i+1,j+1}|0\rangle
\end{aligned}$$

So we obtain the relation:

$$T_x T_y |\psi_{m,n}\rangle = e^{i(\theta^x_{m,n+1} + \theta^y_{m,n})} \hat{c}^\dagger_{i+1,j+1}|0\rangle = e^{i2\pi\phi_{m,n}} T_y T_x |\psi_{m,n}\rangle$$

Even in an external, constant magnetic field, we see that the Hamiltonian is not translationally invariant with the original translational operator because the two don't commute, each other. Even though the magnetic field is translationally invariant, the gauge potential is not.
A gauge transformation is required to make the Hamiltonian translationally invariant, but we will see that we cannot maintain the translational symmetry of the original lattice.

We can find operators that commute with the Hamiltonian, $\tilde{T}_x$ and $\tilde{T}_y$, they are called the magnetic translation operators and are defined by

$$\begin{cases} \tilde{T}_x = \sum_{m,n} \hat{c}^\dagger_{m+1,n} \hat{c}_{m,n} e^{i\chi^x_{m,n}} \\ \tilde{T}_y = \sum_{m,n} \hat{c}^\dagger_{m,n+1} \hat{c}_{m,n} e^{i\chi^y_{m,n}} \end{cases}$$

We could have guessed the form of these operators on physical grounds: they have to be one-body operators because we are solving a one-body Hamiltonian. We also knew that they must have phases that are different from the original ones, because those do not commute. We find the phases χ by requiring that the operators commute with the Hamiltonian, which is a sum of the translation operators in the x and y directions.
Now we impose the following commutation rules in order to find an Hamiltonian that is translationally invariant.

$$\begin{cases} \left[\tilde{T}_x, T_x\right] &= 0 \\ \left[\tilde{T}_x, T_y\right] &= 0 \\ \left[\tilde{T}_y, T_x\right] &= 0 \\ \left[\tilde{T}_y, T_y\right] &= 0 \end{cases}$$

They respectively lead to the following equations, using the method reported in 2.1:

$$\begin{cases} \Delta_x \chi^x_{m,n} = \Delta_x \theta^x_{m,n} \\ \Delta_y \chi^x_{m,n} = \Delta_x \theta^y_{m,n} = \Delta_y \theta^x_{m,n} + 2\pi\phi_{m,n} \\ \Delta_x \chi^y_{m,n} = \Delta_y \theta^x_{m,n} = \Delta_x \theta^y_{m,n} - 2\pi\phi_{m,n} \\ \Delta_y \chi^y_{m,n} = \Delta_y \theta^y_{m,n} \end{cases}$$

The constraints can be solved with the solutions:

$$\begin{aligned} \chi^x_{m,n} &= \theta^x_{m,n} + 2\pi\phi_{m,n} n \\ \chi^y_{m,n} &= \theta^y_{m,n} - 2\pi\phi_{m,n} m \end{aligned}$$

In fact this solutions leads to

$$\begin{cases} \Delta_x(2\pi\phi_{m,n} n) &= 0 \\ \Delta_y(2\pi\phi_{m,n} n) &= 2\pi\phi_{m,n} \\ \Delta_x(-2\pi\phi_{m,n} m) &= -2\pi\phi_{m,n} \\ \Delta_y(-2\pi\phi_{m,n} m) &= 0 \end{cases}$$

From the following rules:

$$\begin{aligned}\phi_{m+1,n} &= \phi_{m,n}\\ \phi_{m,n+1} &= \phi_{m,n}\\ \Delta_y(\phi_{m,n}n) &= \phi_{m,n+1}(n+1) - \phi_{m,n}n = \phi_{m,n}\\ \Delta_x(\phi_{m,n}m) &= \phi_{m+1,n}(m+1) - \phi_{m,n}m = \phi_{m,n}\end{aligned}$$

We have now found operators that commute with $\mathcal{H}$ but do not commute between themselves:

$$\left[\tilde{T}_x, \tilde{T}_y\right] \neq 0$$

In fact:

$$\tilde{T}_x\tilde{T}_y \left|\psi_{i,j}\right\rangle = e^{i\left(\chi^y_{i,j}+\chi^x_{i,j+1}\right)}\hat{c}^\dagger_{i+1,j+1}\left|0\right\rangle$$

and

$$\tilde{T}_y\tilde{T}_x \left|\psi_{i,j}\right\rangle = e^{i\left(\chi^y_{i+1,j}+\chi^x_{i,j}\right)}\hat{c}^\dagger_{i+1,j+1}\left|0\right\rangle$$

In general, we can find a combination of the translation operators that does commute. This combination depends on the gauge that we pick. We select a Gauge that preserve translation symmetry along the $\hat{\mathbf{y}}$ direction $A_y = Bx = 2\pi\phi m$ where ϕ is the uniform flux per plaquette. Hence, from the the Peierls relation, we've $\theta^y_{m,n} = 2\pi\phi m(n+1-n) = 2\pi\phi m$ and the new phases are:

$$\begin{aligned}\chi^x_{m,n} &= 2\pi\phi n\\ \chi^y_{m,n} &= 0\end{aligned}$$

and the relation between the commutators reads as:

$$\tilde{T}_x\tilde{T}_y = e^{i2\pi\phi}\tilde{T}_y\tilde{T}_x$$

By q-successive application of $\tilde{T}_x$ to the preceding relation, we find:

$$\tilde{T}^q_x\tilde{T}_y = e^{i2\pi\phi q}\tilde{T}_y\tilde{T}^q_x$$

and, in general, no power of the magnetic translation operators commutes with the other translation operator. However, for the special case of rational flux per plaquette, $\phi = \frac{p}{q}$ as in the case of golden ratio where $\tau \simeq \frac{F_{i-1}}{F_i}$ where F_i and F_{i-1} are relatively prime we then find that:

$$\tilde{T}^q_x\tilde{T}_y = \tilde{T}_y\tilde{T}^q_x$$

We hence have two operators which commute between themselves and commute with the Hamiltonian; hence, they define a new set of good quantum numbers. In the gauge chosen here, $\tilde{T}_y = \sum_{m,n}\hat{c}^\dagger_{m,n+1}\hat{c}_{m,n}$ is the non-covariantized translation operator, whereas $\tilde{T}_x = \sum_{m,n}\hat{c}^\dagger_{m+1,n}\hat{c}_{m,n}e^{i2\pi\phi n}$. So, we can rewrite the new Hamiltonian as

$$\mathcal{H} = t\sum_{m,n}\hat{c}^\dagger_{m+1,n}\hat{c}_{m,n} + \frac{\lambda}{2}\sum_{m,n}\hat{c}^\dagger_{m,n+1}\hat{c}_{m,n}e^{i2\pi\phi m}$$

Now we apply a Fourier transformation:

$$\hat{c}_{m,n} = \frac{1}{N_y}\sum_{k_y} e^{-ik_y n}\hat{c}_{m,k_y}$$

So the Hamiltonian reads as:

$$\begin{aligned}
\mathcal{H} &= t\sum_{m,n}\left(\frac{1}{N_y}\sum_{k_y'} e^{ik_y^i n}\hat{c}^\dagger_{m+1,k_y'}\frac{1}{N_y}\sum_{k_y''} e^{-ik_y'' n}\hat{c}_{m,k_y''} + h.c.\right) + \\
&\frac{\lambda}{2}\sum_{m,n}\sum_{k_y' k_y''}\left(\frac{1}{N_y}\sum_{k_y} e^{ik_y'(n+1)}\hat{c}^\dagger_{m,k_y'}\frac{1}{N_y}\sum_{k_y''} e^{-ik_y'' n}\hat{c}_{m,k_y''}e^{i2\pi\phi m} + h.c.\right) \\
&= t\sum_m\left(\sum_{k_y'}\hat{c}^\dagger_{m+1,k_y'}\sum_{k_y''}\hat{c}_{m,k_y''}\delta_{k_y',k_y''} + h.c.\right) + \frac{\lambda}{2}\sum_m\sum_{k_y' k_y''}\left(\sum_{k_y}\hat{c}^\dagger_{m,k_y'}\sum_{k_y''}\hat{c}_{m,k_y''}e^{i(2\pi\phi m + k_y')} + h.c.\right) \\
&= t\sum_{m,k_y}\left(\hat{c}^\dagger_{m+1,k_y}\hat{c}_{m,k_y} + h.c.\right) + \lambda\sum_{m,k_y}\hat{c}^\dagger_{m,k_y}\hat{c}_{m,k_y}\cos(2\pi\phi m + k_y)
\end{aligned}$$

where we used the fact that $\sum_n e^{i(k_y' - k_y'')n} = N\delta_{k_y',k_y''}$.
Now we can identify $\hat{c}_{m,k_y} = \hat{c}_{m,k_y}$ and $k_y = \theta$ an arbitrary phase and summing over k_y we obtain the Aubry-André hamiltonian in the real space:

$$\mathcal{H} = t\sum_n\left(\hat{c}^\dagger_{n+1}\hat{c}_n + h.c.\right) + \lambda\sum_n\hat{c}^\dagger_n\hat{c}_n\cos(2\pi\phi n + \theta)$$

In order to obtain the Hamiltonian in the reciprocal space we choose a different Landau Gauge that preserve the flux in $\hat{\mathbf{x}}$-direction: $A_x = By = -2\pi\phi n$ where ϕ is the uniform flux per plaquette. So we obtain

$$\mathcal{H} = t\sum_{m,n}\hat{c}^\dagger_{m+1,n}\hat{c}_{m,n}e^{i2\pi\phi n} + \frac{\lambda}{2}\sum_{m,n}\hat{c}^\dagger_{m,n+1}\hat{c}_{m,n}$$

and after make a Fourier transformation:

$$\hat{c}_{m,n} = \frac{1}{N_x}\sum_{k_x} e^{-ik_x m}\hat{c}_{k_x,n}$$

We obtain:

$$\mathcal{H} = 2t\sum_n\hat{c}^\dagger_n\hat{c}_n\cos(2\pi\phi n + \theta) + \lambda\sum_n\left(\hat{c}^\dagger_{n+1}\hat{c}_n + h.c.\right)$$

The duality is thus identified with two different gauge choices for the Hofstadter problem. We can study the localization properties of the one-dimensional crystal with an incommensurate potential by considering whether the eigenstates of the corresponding two-dimensional crystal in a magnetic field are localized along the $\hat{\mathbf{x}}$-direction, which is the spatial direction in the original one-dimension problem.
When the field strenght $B = \frac{\phi}{2\pi} \ll 1$, the dynamics of Bloch electrons is given semiclassically

by the Lorentz force law:

$$\hbar\frac{\mathrm{d}\mathbf{k}}{\mathrm{d}t} = -e\mathbf{v}(\mathbf{k}) \times \mathbf{B} = \frac{e}{\hbar}\left(\mathbf{B} \times \frac{\mathrm{d}E(\mathbf{k})}{\mathrm{d}\mathbf{k}}\right)$$

where $\mathbf{v}(\mathbf{k}) = \frac{1}{\hbar}\frac{\mathrm{d}E(\mathbf{k})}{\mathrm{d}\mathbf{k}}$ is the electron group velocity.
The resulting electron orbits is defined by the zero-field energy dispersion $E = \epsilon_k = 2t\cos(k_x) + \lambda\cos(k_y)$.
Since the velocity of an electron is perpendicular to the constant energy contour, the semiclassical motion is localized in the $\hat{\mathbf{x}}$ direction unless the countour is open along the k_y direction, which occurs when $\lambda < 2t - |E|$.
This seemingly implies that for amplitude $\lambda < 2t$ there are two mobilities edges at $E_{c,\pm} = \pm(2t - \lambda)$ ([19]); the states are de-localized between these energies, while all states beyond the mobility edges are localized. Meanwhile for $\lambda > 2t$ all states are localized.
The wave vector τ in Harper's equation plays the role of a magnetic field in the two dimensional scenario. For $B = \tau \ll 1$, the semiclassical results are expected to be asymptotically exact, and the transition should be almost independent of τ.

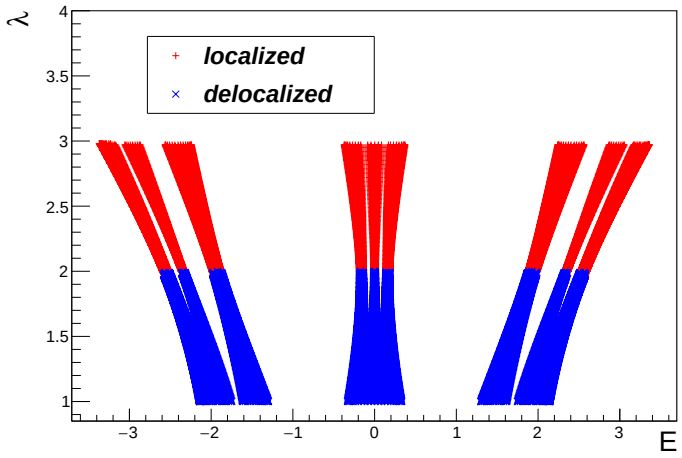

Figure 2.1: The Phase diagram for Aubry-Andrè model with τ equal to golden ratio obtained from numerical study of IPR-function on a system of size $L = 1000$.

2.2 Numerical Calculations

The fractal dimension is a way to characterizing the wave functions in disordered systems [20], [21].
The quantity D can be defined if the integral of the probability density $|\psi(\mathbf{r})|^2$ within a sphere of radius L is proportional to L^D with D independent of L.
$\psi(\mathbf{r})$ is the normalized wave function of the disordered system under consideration. For a disordered eigenfunction the result dependent strongly on where the center of the sphere is placed. To avoid this difficult a weighted average over all positions of the center is taken.

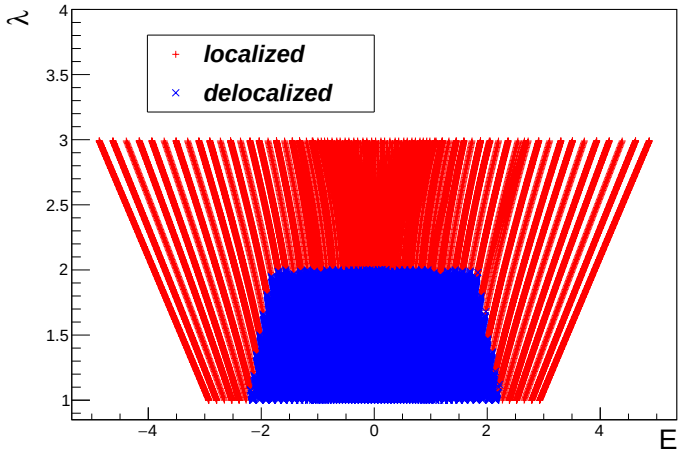

Figure 2.2: The Phase diagram for Aubry-Andrè model with $\tau = \frac{\sqrt{5}+1}{2}0.01$ obtained from numerical study of IPR-function on a system of size $L = 1000$.

The weight is the probability density of finding the particle at each point. Thus the fractal dimensionality was defined as the L-independent exponent in the relation $A(L) \propto L^D$ where $A(L)$ is the density correlation function defined by:

$$A(L) := \int d\mathbf{r}|\psi(\mathbf{r})|^2 \int_0^L d\mathbf{r}'|\psi(\mathbf{r}+\mathbf{r}')|^2$$

In the 1D case this function can be discretized as

$$A(L) := \sum_{j=1}^{L'} |\psi(j)|^2 \sum_{i=1}^{L} |\psi(i+j)|^2$$

where L' is the site number of the chain.
For uniform extended states, the fractal dimensionality coincides with the Euclidean dimensionality $D = d$. *Zdetsis et al*, in [20], calculated the fractal dimensionality D as a function of λ. They took $E = 0$ as the energy under consideration in their work.
They found for $\lambda < 1.95t$, $D = 1$, while for $\lambda > 2.05t$ D drops below 0.5. At the critical point $\lambda = 2t$, we estimate $D = 0.80 \pm 0.15$ independent of E and τ.
We show that this result was misleading in the limit for $\tau \to 0$ but also for $\tau \simeq 1$.
The fractal dimension is defined into critical point $\lambda_c = 2t$.
We have calculated the IPR-function for each energy of the system. After choosing a IPR-threshold defined by the value at $\lambda_c = 2$ and $E \simeq 0$, we have discriminated localized states from delocalized states based on the value of the eigenstates IPR-function.
So if this value is greater than the threshold the state is localized, otherwise the state is delocalized.
We have made the phase diagrams for the value of $\tau = \frac{\sqrt{5}+1}{2}$ in figure 2.1, $\tau = \frac{\sqrt{5}+1}{2}0.001$ in figure 2.2 and $\tau = \frac{\sqrt{5}+1}{2}0.001$ in figure 2.3.
The results obtained tell us that exist states more localized than others for $\lambda < 2$ and also

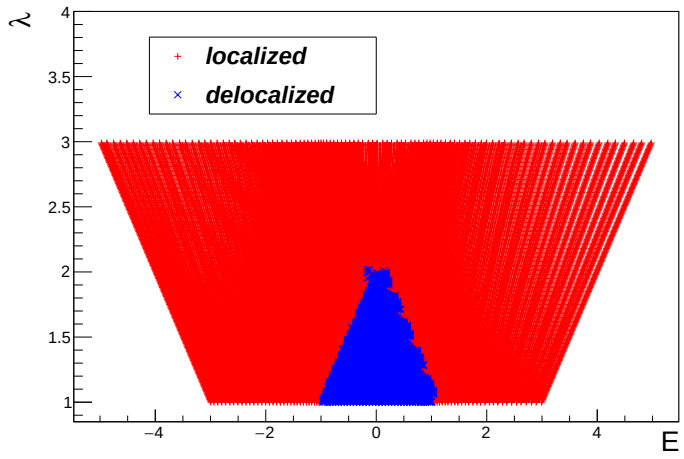

Figure 2.3: The Phase diagram for Aubry-Andrè model with $\tau = \frac{\sqrt{5}+1}{2} 0.001$ obtained from numerical study of IPR-function on a system of size $L = 1000$.

for $\lambda = 2$. In particular we have seen that the ground-state state is more localized than the $E \simeq 0$ state (figure 2.4). We have considered a lattice with 5000 sites for $\lambda_c = 2$ and we plot $\ln A(L)$ versus the number of the site. The angular coefficient of this curve will be the fractal dimension of this system.
We have found, taken ground-state energy as the energy under consideration, $D_{gs} = 0.442922 \pm 0.00331461$, as it can see in figure 2.6. The result, reported in [20], takes agree with us for $E \simeq 0$ as $D_0 = 0.785705 \pm 0.0155619$.
We verify also the fractal dimension for delocalized states for $\lambda = 1.50 < \lambda_c$ in figure 2.7. In this case the fractal dimension is $D = 1.0392 \pm 0.00179431$, like [20] suggested.

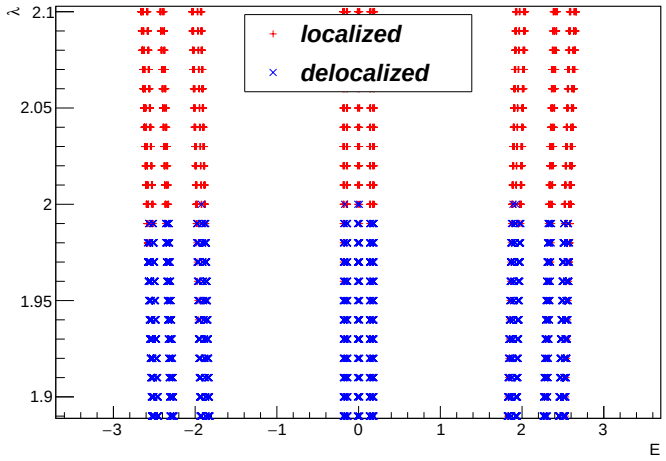

Figure 2.4: Zoom of figure 2.1

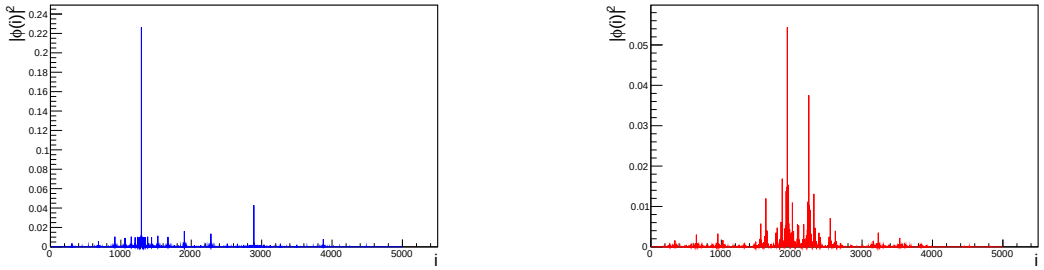

Figure 2.5: Square of the wavefunction versus lattice site i for $\lambda = 2$ for a system of size $L = 5000$, E_{gs} in blue line (left side) and $E \simeq 0$ in red line (right side).

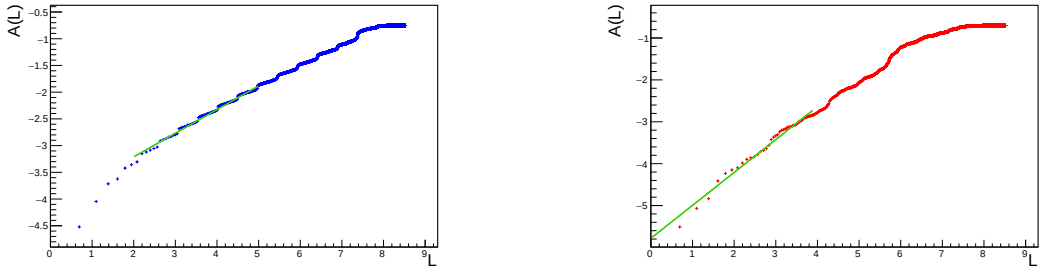

Figure 2.6: Logarithm of the density correlation function $A(L)$ versus the lattice site i for a system of size $L = 5000$. $A(L)$ is calculated for $\lambda = 2$, E_{gs} in blue line and $E \simeq 0$ in red line.

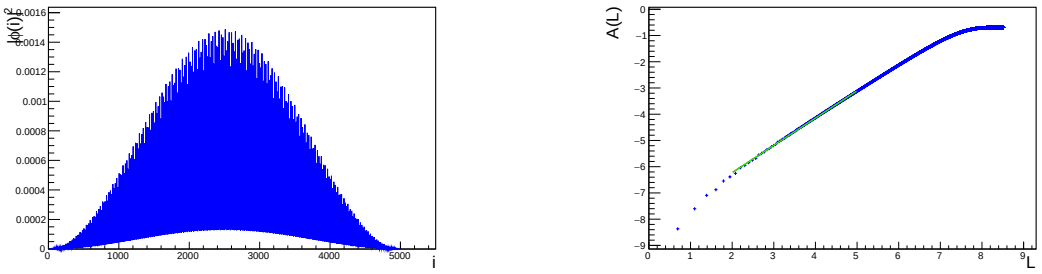

Figure 2.7: Logarithm of the density correlation function $A(L)$ versus the lattice site i for a system of size $L = 5000$. $A(L)$ is calculated for $\lambda = 1.50$ and E_{gs}.

Chapter 3

Next-nearest neighbors and the appearance of mobility edge

In this chapter we study the effects on the localization transition of the next-nearest-neighbors (NNN) hopping in the Aubry-André Model [18].
We will show, analytically and numerically, the dependence of the critic quasi-disorder strength λ_c from NNN hopping t_2 and in particular the energy dependent mobility edges.

3.1 Numerical method

We consider a single particle moving, towards NN and NNN hopping matrix elements, in a one-dimensional optical lattice with Aubry-André potential.
The Hamiltonian of this system is:

$$\mathcal{H} = \sum_{i,j}^{L} \left(t_1 \hat{b}_i^\dagger \hat{b}_{i+j} + t_2 \hat{b}_i^\dagger \hat{b}_{i+2j} \right) + \sum_{i}^{L} \epsilon_i \hat{b}_i^\dagger \hat{b}_i$$

where i is a site index in a one-dimensional optical lattice with a lattice constant a, t_1 and t_2 are the NN and NNN hopping matrix elements respectively, $\epsilon_n = \lambda \cos(2\pi q n)$ is energy in situ, $\hat{b}_i$ is an annihilation operator for a particle at site i, $j = \pm 1$ is the locator of a NN site, λ is the strength of the AA potential, and $q = \frac{\sqrt{5}+1}{2}$ is the incommensurable parameter. The eigenvalue equation is:

$$t_1 \left(u_{n-1} + u_{n+1} \right) + t_2 \left(u_{n-2} + u_{n+2} \right) + \epsilon_n u_n = E u_n$$

where u_n is the amplitude of the wave function at site n and E the energy eigenvalue. The system, how we've seen in chapter 1, is invariant for $t_1 \mapsto t_1' = -t_1$. So we can rescale all the energies in units of $|t_1|$. The parameters remain t_2 and λ.
The eigenvalue equation becomes:

$$\left(u_{n-1} + u_{n+1} \right) + t_2 \left(u_{n-2} + u_{n+2} \right) + \epsilon_n u_n = E u_n$$

Numerically we have solved the equation:

$$\mathcal{H}_n u_n = E u_n$$

where:

$$\mathcal{H}_n = \begin{bmatrix} \epsilon_1 & 1 & t_2 & 0 & \dots & \dots & \dots & \dots & 0 \\ 1 & \epsilon_2 & \ddots & \ddots & \ddots & \ddots & \ddots & \ddots & \vdots \\ t_2 & 1 & \epsilon_3 & \ddots & \ddots & \ddots & \ddots & \ddots & \vdots \\ 0 & \ddots & \ddots & \ddots & \ddots & \ddots & \ddots & \ddots & \vdots \\ \vdots & \ddots & \ddots & \ddots & \ddots & \ddots & \ddots & \ddots & \vdots \\ 0 & \dots & 0 & t_2 & 1 & \epsilon_{n-3} & 1 & t_2 & 0 \\ 0 & \dots & \dots & 0 & t_2 & 1 & \epsilon_{n-2} & 1 & t_2 \\ 0 & \dots & \dots & \dots & 0 & t_2 & 1 & \epsilon_{n-2} & 1 \\ 0 & \dots & \dots & \dots & \dots & 0 & t_2 & 1 & \epsilon_n \end{bmatrix}$$

We monitor the localization properties by calculating the Shannon entropy and the IPR-function, defined in chapter 1.

In figure 3.1 we show the variations of the S and IPR of the ground state as a function of

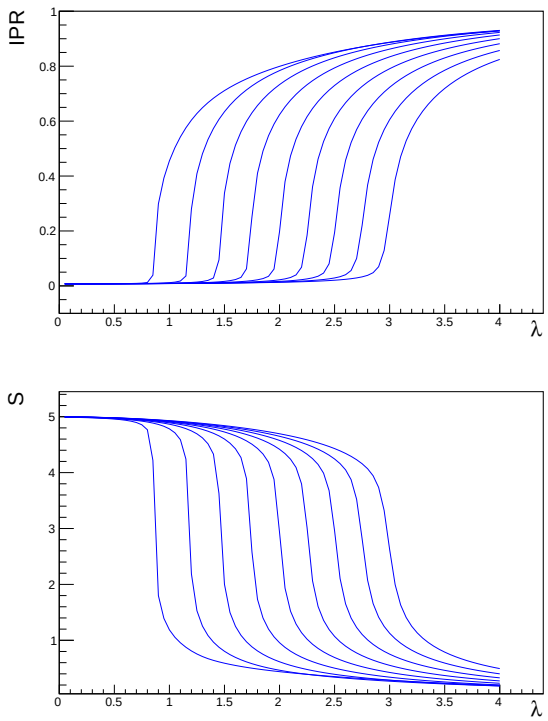

Figure 3.1: Shannon Entropy and the IPR as a function of the AA quasi-disorder potential strength λ for a open chain with 200 lattice sites for different values of t_2 . From left to right, the curves are for $t_2 = 0.2$, 0.15, 0.1, 0.05, 0, -0.05, -0.1, -0.15, and -0.2, respectively.

the quasi-disorder strength for various values of t_2. The transition from the extended to the localized state is signaled by a large drop in S and a large rise in IPR.

In the absence of t_2 the transition occurs at a critical disorder strength $\lambda_c = 2$, as we have seen in the chapter 1. It is seen that λ_c changes as t_2 is introduced and the sign of t_2 has a significant effect on the localization transition. The λ_c for the ground state decreases with $|t_2|$

for t_2 positive and increases with $|t_2|$ for t_2 negative. Numerically we've seen that the result doesn't depend by the sign of t_1.

Next we have studied the energy dependence of the λ_c. We have numerically obtained the λ_c for all the 2330 eigenstates from the calculations of the $\frac{dS}{d\lambda}$ as well as the $\frac{dIPR}{d\lambda}$ as a function of λ as shown in figure 3.4 for two states. For each eigenstate, the value of λ for which $\frac{dS}{d\lambda}$ is minimum and $\frac{dIPR}{d\lambda}$ is maximum is taken as the λ_c of that state and the corresponding eigenenergy is E_c . We note here that $\frac{dS}{d\lambda}$ is a better indicator of the localization transition compared to $\frac{dIPR}{d\lambda}$.
We plotted in the figure 3.2 the variation of the λ_c for $t_2 = 0.1$ and $t_2 = -0.1$. The λ_c is seen to increase approximately linearly with increasing energy. It may be noted that for positive t_2 this trend is reverse.

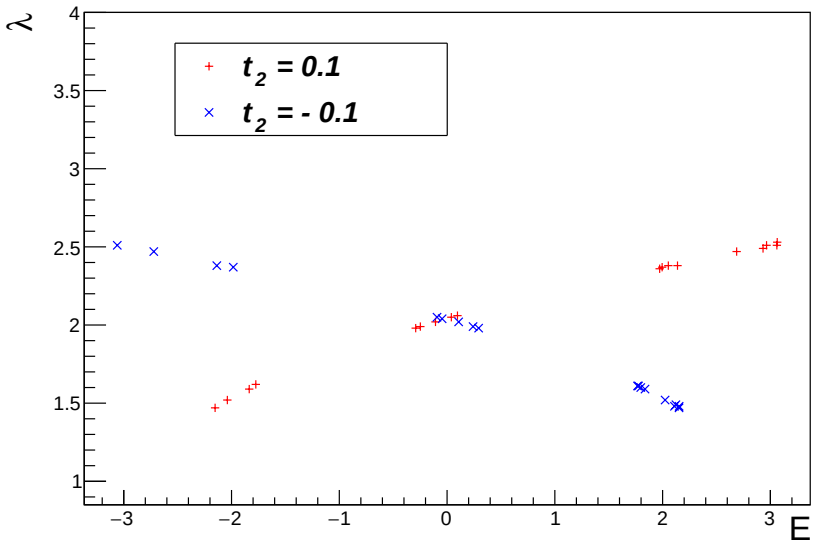

Figure 3.2: Plot of λ_c vs E_c for $t_2 = 0.1$ (blue x marker) and $t_2 = -0.1$ (red plus marker). The points represent numerically determined λ_c and energy eigenvalues for different eigenstates for a closed chain of 2000 lattice sites.

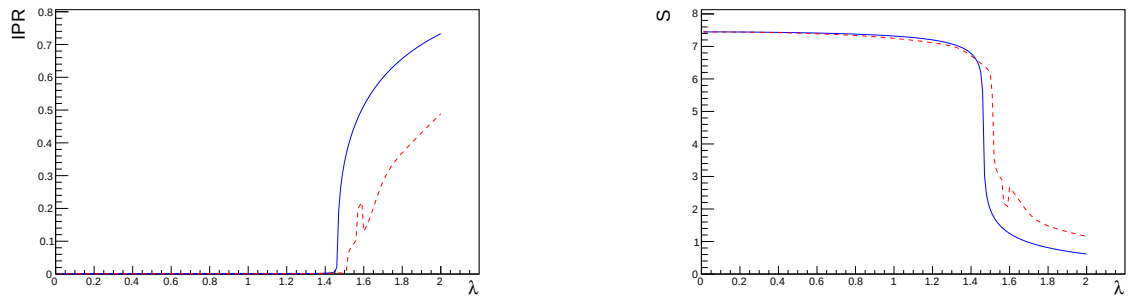

Figure 3.3: Shannon Entropy and the IPR as a function of the AA quasi-disorder potential strength λ for the ground state (blue continue line) and 390th excited state (red dashed line) of a particle in a lattice with 2330 sites and $t_2 = 0.1$

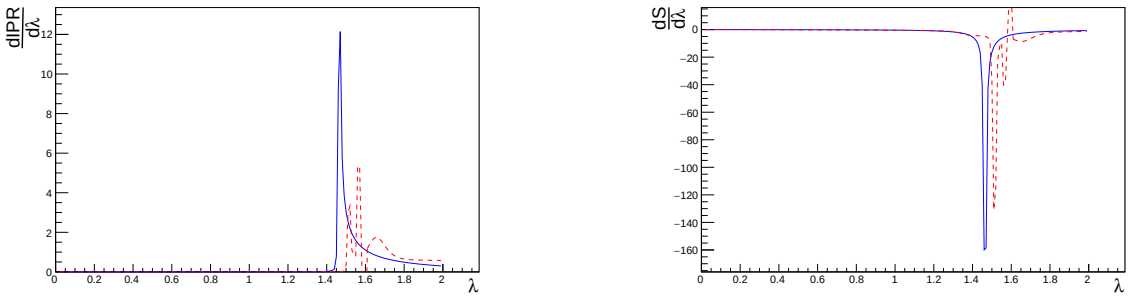

Figure 3.4: The variation of $\frac{dS}{d\lambda}$ and $\frac{dIPR}{d\lambda}$ with λ for the ground state (blue continue line) and 390th excited state (red dashed line) of a particle in a lattice with 2330 sites and $t_2 = 0.1$

3.2 Analytical Calculations

The numerical results can be understood from an extension of analytical calculations given in [22].
We consider the following Hamiltonian for an infinite system:

$$\mathcal{H} = \sum_{n,n'}{}' t_{nn'} \hat{b}_n^\dagger \hat{b}_{n'} + \lambda \sum_n \cos(2\pi q n) \hat{b}_n^\dagger \hat{b}_n$$

where $\sum'_{n,n'} := \sum_{n,n'}(1 - \delta_{n,n'})$, and the generalized hopping term is

$$t_{nn'} := e^{is\pi} t e^{-(p+is\pi)|n-n'|}$$

n and n' are the site index, $s = 0, 1$ and p an arbitrary positive parameter. Here, the hopping strength decreases exponentially with increasing distance and our choice makes t_1 positive whereas t_2 is positive or negative depending on $s = 0$ or 1.
So

$$t_1 := t_{n,n+1} = te^{-p}$$

whereas

$$t_2 := t_{n,n+2} = te^{-is\pi} e^{-2p}$$

We rewrite the Hamiltonian hopping term as:

$$\sum_{n,n'}{}' t_{nn'} \hat{b}_n^\dagger \hat{b}_{n'} = \sum_{n,n'} t_{nn'} \hat{b}_n^\dagger \hat{b}_{n'} - \sum_n \hat{b}_n^\dagger \hat{b}_n$$

Hence the eigenvalue equation is:

$$\left(E + e^{is\pi} t - \lambda \cos(2\pi q n)\right) u_n = e^{is\pi} \sum_{n'} t e^{-(p+is\pi)|n-n'|} u_{n'} \tag{3.1}$$

where u_n is the amplitude of the wave function at site n and E the energy eigenvalue.
Now we define the following quantities:

$$\cosh(p_0) = e^{is\pi} \left(\frac{E + e^{is\pi} t}{\lambda} \right)$$

which gives

$$\sinh(p_0) = \sqrt{\cosh(p_0)^2 - 1} = \frac{\omega}{\lambda} e^{is\pi}$$

where

$$\omega = \sqrt{(E + e^{is\pi} t)^2 - \lambda^2}$$

and

$$T_n(p_0) := \frac{\cosh(p_0) - e^{is\pi} \cos(2\pi q n)}{\sinh(p_0)}$$

We can note that

$$\begin{aligned}\omega T_n(p_0) &= \frac{\lambda}{e^{is\pi}}\sinh(p_0)\frac{\cosh(p_0)-e^{is\pi}\cos(2\pi qn)}{\sinh(p_0)}\\ &= \lambda e^{-is\pi}\cosh(p_0)-\lambda\cos(2\pi qn)\\ &= E+e^{is\pi}t-\lambda\cos(2\pi qn)\end{aligned}$$

is exactly the first member on the eigenvalue equation 3.1. Hence the eigenvalue equation can be write as:

$$\omega T_n(p_0)u_n = e^{is\pi}\sum_{n'} te^{-(p+is\pi)|n-n'|}u_{n'}$$

Now we multiply both sides of it with $T_m(p)e^{imn2\pi q}$ and summing over n. The first member becomes:

$$\omega T_m(p)\sum_n e^{imn2\pi q}T_n(p_0)u_n = \omega T_m(p)\tilde{u}_m$$

where

$$\tilde{u}_m \coloneqq \sum_n e^{imn2\pi q}T_n(p_0)u_n$$

is the amplitude of the wave function at site n in the reciprocal space. Meanwhile the second member evolves to:

$$e^{is\pi}tT_m(p)\sum_n e^{imn2\pi q}\sum_{n'} e^{-(p+is\pi)|n-n'|}u_{n'}$$

We put $r \coloneqq n-n'$, $n = r+n'$ obtaining:

$$e^{is\pi}tT_m(p)\sum_r e^{imr2\pi q}e^{-(p+is\pi)|r|}\sum_{n'} e^{imn'2\pi q}u_{n'}$$

Now we have this identity, demonstrated explicitly in Appendix B:

$$T_m(p)^{-1} = \sum_r e^{-(p+is\pi)|r|}e^{imr2\pi q}$$

The second member is reduced to:

$$e^{is\pi}t\sum_{n'} e^{imn'2\pi q}u_{n'}$$

In the sum we insert the term $T_{n'}(p_0)^{-1}T_{n'}(p_0)$:

$$\begin{aligned}e^{is\pi}t\sum_{n'} e^{imn'2\pi q}u_{n'} &= e^{is\pi}t\sum_{n'} T_{n'}(p_0)^{-1}T_{n'}(p_0)e^{imn'2\pi q}u_{n'}\\ &= \sum_{r,n'} e^{-(p_0+is\pi)|r|}e^{2\pi in'rq}T_{n'}(p_0)e^{imn'2\pi q}u_{n'}\\ &= \sum_{r,n'} e^{-(p_0+is\pi)|r|}e^{2\pi in'(r+m)q}T_{n'}(p_0)u_{n'}\end{aligned}$$

where in the second passage we explicitly write the $T_{n'}(p_0)^{-1}$ term.
Now we put $m' \coloneqq r + m$,$r = m' - m$:

$$\sum_{m'} e^{-(p_0+is\pi)|m'-m|} \sum_{n'} e^{2\pi i n' m' q} T_{n'}(p_0) u_{n'} = \sum_{m'} e^{-(p_0+is\pi)|m'-m|} \tilde{u}_{m'}$$

Finally we get two different equations that become self dual for $p = p_0$. Now we conjecture, following the Aubry-André work, that all states are localized for $p > p_0$ and delocalized for $p < p_0$. With this assumption the amplitude wave functions u_n and $\tilde{u}_n$ are respectively localized and delocalized for $p > p_0$; viceversa for $p < p_0$.

$$\omega T_n(p_0) u_n = e^{is\pi} \sum_{n'} t e^{-(p+is\pi)|n-n'|} u_{n'}$$
$$\omega T_n(p) \tilde{u}_n = e^{is\pi} \sum_{n'} t e^{-(p_0+is\pi)|n-n'|} \tilde{u}_{n'}$$

At the self dual point λ_c we get $\cosh(p) = \cosh(p_0)$. Hence we have the following equality:

$$\cosh(p) = e^{is\pi} \left(\frac{E + e^{is\pi} t}{\lambda_c} \right)$$

Making clear all terms we have

$$\begin{aligned} \lambda_c &= e^{is\pi} \left(\frac{E + e^{is\pi} t}{\cosh(p)} \right) \\ &= \frac{2e^{-p} E e^{is\pi} + 2e^{-p} t}{1 + e^{-2p}} \end{aligned}$$

Remembering that $t_1 = te^{-p}$ and $t_2 = te^{-is\pi} e^{-2p}$, we obtain:

$$\lambda_c = \frac{2t_1 + 2E\left(\frac{t_2}{t_1}\right)}{1 + \left(\frac{t_2}{t_1}\right)^2}$$

When $t_2 = 0$, the critical disorder strength λ_c is energy independent and is equal to $2t_1$, a result obtained for the original AA model. When $t_2 \neq 0$ and energy E is fixed, the change in λ_c is proportional to t_2 provided $\frac{t_2}{t_1}$ is small. For a fixed value of t_2, λ_c increases or decreases linearly with the energy eigenvalue E depending on t_2 being positive or negative.

3.3 Phase Diagram

Relying on the numerical and approximate analytical calculations we built the phase diagram for this model. In the same way as chapter 1 we have calculated the IPR-function for each energy of the system. After choosing a IPR-threshold defined by the value at $\lambda_c = 2.04$ and $E \simeq 0$, where we have found numerically a localization transition, we have discriminated localized states from delocalized states based on the value of the eigenstates IPR-function. So if this value is greater than the threshold the state is localized, otherwise the state is

delocalized. This procedure leads to the figures 3.5 and 3.6.
The numerical results are in reasonable agreement with the analytical results. Note that the numerical results are obtained considering NN and NNN hopping terms only while the analytical results are derived considering long range hopping which decays exponentially with distance. We find that an increase in $|t_2|$ for negative t_2 increases the λ_c while increasing positive t_2 reduces λ_c and that it decreases almost linearly with increasing t_2. We find also that for $|t_2| \neq 0$ the energy spectrum isn't symmetric respect λ axis (figures 3.5 and 3.6).

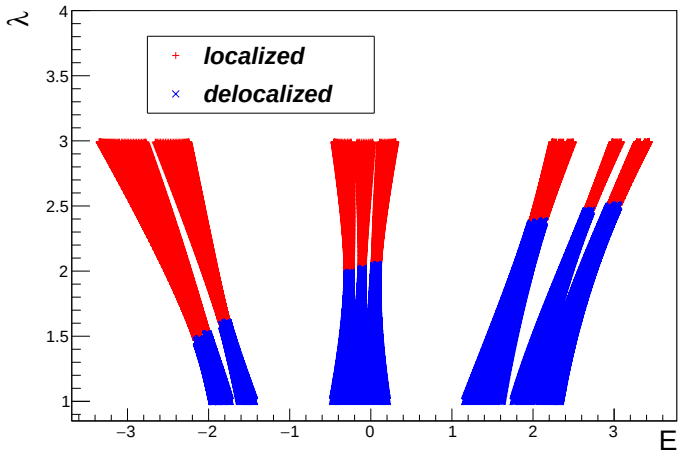

Figure 3.5: The Phase diagram for Aubry-Andrè model with NNN hopping term $t_d = 0.1$ obtained from numerical study of IPR-function on a system of size $L = 2000$.

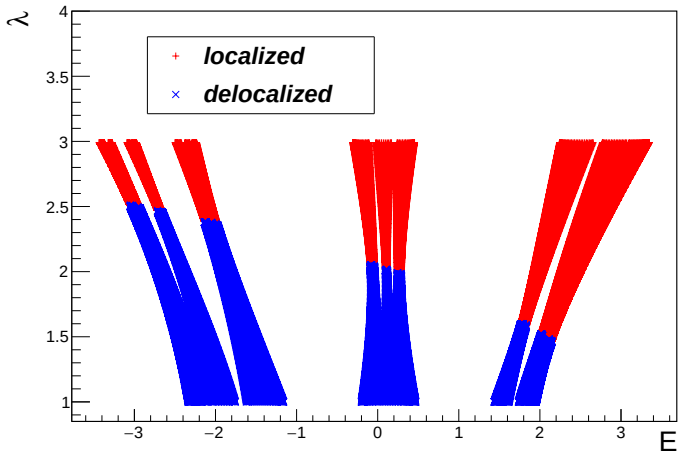

Figure 3.6: The Phase diagram for Aubry-Andrè model with NNN hopping term $t_d = -0.1$ obtained from numerical study of IPR-function on a system of size $L = 2000$.

Chapter 4

From a particular chain to two coupled chains

In this chapter we throw the basis and the ideas to build a quasi-1d system composed by two Aubry-André chains coupled with a transversal hopping term.

4.1 A general Hamiltonian for two coupled chains

We consider the following schematic view of two coupled chains:

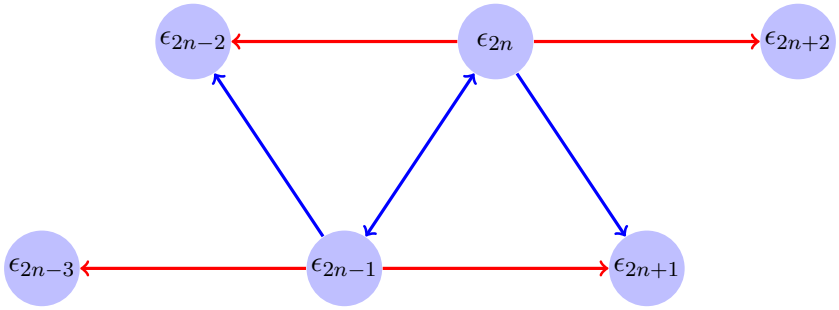

where the energies satisfy the following equality:

$$\epsilon_{2n} = \epsilon_{2n-1} \qquad \forall n \tag{4.1}$$

We want derive the Hamiltonian of this system from a particular Aubry-André 1d chain with the coupling parameter between chains as the NN hopping, the hopping coefficient between the site of the same chain as the NNN hopping and the on-site potential satisfy the constraint 4.1.
Let's start from the following Hamiltonian:

$$\mathcal{H} = \sum_{n,n'}{}' t_{n,n'} \hat{b}_n^\dagger \hat{b}_{n'} + \lambda \sum_n \cos(kg(n)) \hat{b}_n^\dagger \hat{b}_n$$

where $\sum'_{n,n'} \coloneqq \sum_{n \neq n'}$ and

$$kg(n) \coloneqq \frac{\pi q}{2}\left[2n + 1 - (-1)^n\right]$$

The $kg(n)$ function ensure that the constraint 4.1 is satisfied.
Now we rewrite the hopping matrix elements term as

$$\sum_{n,n'}{}' t_{nn'}\hat{b}_n^\dagger \hat{b}_{n'} = \sum_{n,n'} t_{nn'}\hat{b}_n^\dagger \hat{b}_{n'} - t_{n,n}\sum_n \hat{b}_n^\dagger \hat{b}_n$$

and substitute it in the Hamiltonian:

$$\mathcal{H} = \sum_{n,n'} t_{nn'}\hat{b}_n^\dagger \hat{b}_{n'} - t_{n,n}\sum_n \hat{b}_n^\dagger \hat{b}_n + \lambda \sum_n \cos(kg(n))\hat{b}_n^\dagger \hat{b}_n$$

We want identify two different operators that act on different chain sites. In other words we want build an operator for the first chain and an operator for the second chain. This imply that these operators commute with each other.
In order to obtain it, we separate the even and odd terms of the two indices n, n':

$$\begin{aligned}\mathcal{H} = \sum_{n,n'} \Big(t_{2n,2n'}\hat{b}_{2n}^\dagger \hat{b}_{2n'} + t_{2n,2n'-1}\hat{b}_{2n}^\dagger \hat{b}_{2n'-1} + t_{2n-1,2n'}\hat{b}_{2n-1}^\dagger \hat{b}_{2n'} + t_{2n-1,2n'-1}\hat{b}_{2n-1}^\dagger \hat{b}_{2n'-1}\Big) + \\ -t_{n,n}\sum_n \left(\hat{b}_{2n}^\dagger \hat{b}_{2n} + \hat{b}_{2n-1}^\dagger \hat{b}_{2n-1}\right) + \lambda \sum_n \cos(kg(2n))\left(\hat{b}_{2n}^\dagger \hat{b}_{2n} + \hat{b}_{2n-1}^\dagger \hat{b}_{2n-1}\right)\end{aligned}$$

In the last term we use the constraint 4.1.
Now we impose the hermitianicity of the Hamiltonian. This request implies in particular that:

$$\sum_{n,n'} t_{2n-1,2n'}\hat{b}_{2n-1}^\dagger \hat{b}_{2n'} + t_{2n-1,2n'-1}\hat{b}_{2n-1}^\dagger \hat{b}_{2n'-1} = \sum_{n,n'} \Big(t_{2n-1,2n'}\hat{b}_{2n-1}^\dagger \hat{b}_{2n'} + t_{2n-1,2n'-1}\hat{b}_{2n-1}^\dagger \hat{b}_{2n'-1}\Big)^\dagger$$

and the following constraints:

$$\begin{cases} t_{2n',2n-1} &= t_{2n-1,2n'} \\ t_{2n'-1,2n} &= t_{2n,2n'-1} \end{cases}$$

So we can rewrite the Hamiltonian as:

$$\begin{aligned}\mathcal{H} = \sum_{n,n'} \Big(t_{2n,2n'}\hat{b}_{2n}^\dagger \hat{b}_{2n'} + t_{2n-1,2n'-1}\hat{b}_{2n}^\dagger \hat{b}_{2n'-1}\Big) + t_{2n-1,2n'}\left(\hat{b}_{2n-1}^\dagger \hat{b}_{2n'} + \hat{b}_{2n'-1}^\dagger \hat{b}_{2n}\right) + \\ -t_{n,n}\sum_n \left(\hat{b}_{2n}^\dagger \hat{b}_{2n} + \hat{b}_{2n-1}^\dagger \hat{b}_{2n-1}\right) + \lambda \sum_n \cos(kg(2n))\left(\hat{b}_{2n}^\dagger \hat{b}_{2n} + \hat{b}_{2n-1}^\dagger \hat{b}_{2n-1}\right)\end{aligned}$$

Now we divide the terms in the sums into $n = n'$ and $n \neq n'$. So we obtain:

$$\begin{aligned}\mathcal{H} = \sum_{n \neq n'} \Big(t_{2n,2n'}\hat{b}_{2n}^\dagger \hat{b}_{2n'} + t_{2n-1,2n'-1}\hat{b}_{2n}^\dagger \hat{b}_{2n'-1}\Big) + \sum_{n \neq n'} t_{2n-1,2n'}\left(\hat{b}_{2n}^\dagger \hat{b}_{2n'-1} + \hat{b}_{2n'-1}^\dagger \hat{b}_{2n}\right) + \\ + \sum_n t_{2n-1,2n}\left(\hat{b}_{2n-1}^\dagger \hat{b}_{2n} + \hat{b}_{2n-1}^\dagger \hat{b}_{2n}\right) + \lambda \sum_n \cos(kg(2n))\left(\hat{b}_{2n}^\dagger \hat{b}_{2n} + \hat{b}_{2n-1}^\dagger \hat{b}_{2n-1}\right)\end{aligned}$$

Finally we introduce two operators $\hat{b}_{2n} \coloneqq \hat{c}_n$ and $\hat{b}_{2n-1} \coloneqq \hat{d}_n$ which will identify the first and second chain respectively. Hence a general Hamiltonian that describes our system is:

$$\mathcal{H} = \sum_{n \neq n'} \left(t_{2n,2n'} \hat{c}_n^\dagger \hat{c}_{n'} + t_{2n-1,2n'-1} \hat{d}_n^\dagger \hat{d}_{n'} \right) + \sum_{n \neq n'} t_{2n-1,2n'} \left(\hat{c}_n^\dagger \hat{d}_{n'} + \hat{d}_{n'}^\dagger \hat{c}_n \right) + \\ + \sum_n t_{2n-1,2n} \left(\hat{c}_n^\dagger \hat{d}_n + \hat{d}_n^\dagger \hat{c}_n \right) + \lambda \sum_n \cos(2\pi q n) \left(\hat{c}_n^\dagger \hat{c}_n + \hat{d}_n^\dagger \hat{d}_n \right) \tag{4.2}$$

4.2 Two weak coupled chains: different geometry structure

The aim of this section is to study numerically different geometry structures for two identical weak coupled chains in the regime of Aubry-Andrè Model.
We will present the numerical methods used to define the localization transition and some possible relations with the case of NNN Aubry-André Model.

4.2.1 Triangular lattice

We consider two identical chains, coupled with an hopping term t_d, that simulate a triangular structure. This system can be described by the Hamiltonian 4.2 where we assume $t_{2n,2n'} = t_{2n-1,2n'-1} = 1$ and $t_{2n-1,2n'} = t_d$:

$$\mathcal{H} = \sum_{n,j} \left(\hat{c}_n^\dagger \hat{c}_{n+j} + \hat{d}_n^\dagger \hat{d}_{n+j} \right) + t_d \sum_{n,j} \left(\hat{c}_n^\dagger \hat{d}_{n+j} + \hat{d}_{n+j}^\dagger \hat{c}_n \right) + \\ + t_d \sum_n \left(\hat{c}_n^\dagger \hat{d}_n + \hat{d}_n^\dagger \hat{c}_n \right) + \lambda \sum_n \cos(2\pi q n) \left(\hat{c}_n^\dagger \hat{c}_n + \hat{d}_n^\dagger \hat{d}_n \right)$$

that leads the eigenvalue equation:

$$\mathcal{H}_n u_n = E u_n$$

where

$$\mathcal{H}_n = \left[\begin{array}{c|c} M & R \\ \hline S & M \end{array} \right]$$

The matrix M is:

$$M = \begin{bmatrix} \epsilon_1 & 1 & 0 & \dots & 0 \\ 1 & \epsilon_2 & 1 & \ddots & \vdots \\ 0 & 1 & \epsilon_3 & \ddots & 0 \\ \vdots & \ddots & \ddots & \ddots & 1 \\ 0 & \dots & 0 & 1 & \epsilon_n \end{bmatrix}$$

and R and S are:

$$R = \begin{bmatrix} t_d & 0 & 0 & \dots & 0 \\ t_d & t_d & \ddots & \ddots & \vdots \\ 0 & t_d & t_d & \ddots & 0 \\ \vdots & \ddots & \ddots & \ddots & 0 \\ 0 & \dots & 0 & t_d & t_d \end{bmatrix}$$

$$S = \begin{bmatrix} t_d & t_d & 0 & \dots & 0 \\ 0 & t_d & \ddots & \ddots & \vdots \\ 0 & 0 & t_d & \ddots & 0 \\ \vdots & \ddots & \ddots & \ddots & t_d \\ 0 & \dots & 0 & 0 & t_d \end{bmatrix}$$

In figures 4.1 and 4.2 we have shown the variations of the S and IPR of the ground state

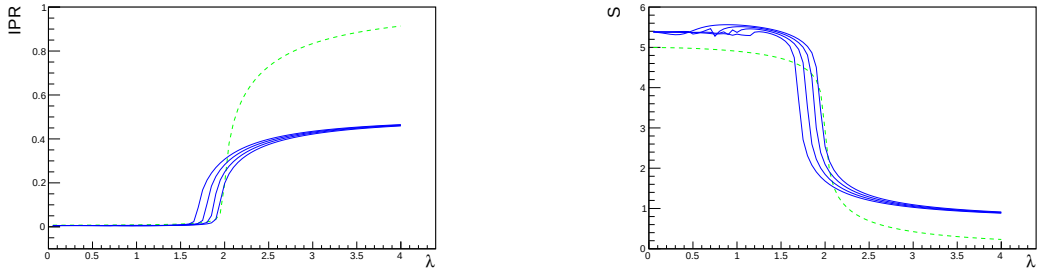

Figure 4.1: Shannon Entropy and the IPR as a function of the AA quasi-disorder potential strength λ for two open chains with 2000 lattice sites each other for different values of t_d . From left to right, the curves are for $t_d = -0.2$, -0.15, -0.1, -0.05 and 0, respectively. The green dashed line identify IPR and Shannon entropy curve for $t_d = 0$.

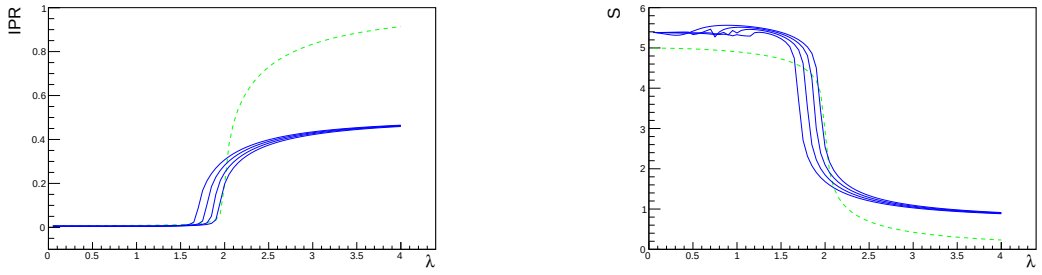

Figure 4.2: Shannon Entropy and the IPR as a function of the AA quasi-disorder potential strength λ for two open chains with 2000 lattice sites each other for different values of t_d . From left to right, the curves are for $t_d = 0.2$, 0.15, 0.1, 0.05 and 0, respectively. The green dashed line identify IPR and Shannon entropy curve for $t_d = 0$.

as a function of the quasi-disorder strength for various values of t_d. The transition from the extended to the localized state is signaled by a large drop in S and a large rise in IPR.
In the absence of t_d the transition occurs at a critical disorder strength $\lambda_c = 2$, as we have seen in the chapter 1. It is seen that λ_c changes as t_d is introduced and the sign of t_d has a significant effect on the localization transition. The λ_c for the ground state decreases with $|t_2|$ and $t = 1$. We may aspect an inverse trend for $t = -1$.
This intuition is based on the fact that t hopping term works as NNN hopping in the model discuss in chapter 3, where we have seen that the trend of λ_c is reverse with NNN hopping sign.

We plotted in the figure 4.3 the variation of the λ_c for $t_d = 0.1$. The λ_c moves approximately inside two different values, which are the ground state critic strength and another λ_c approximately symmetric to the first with the axis $\lambda = 2$.

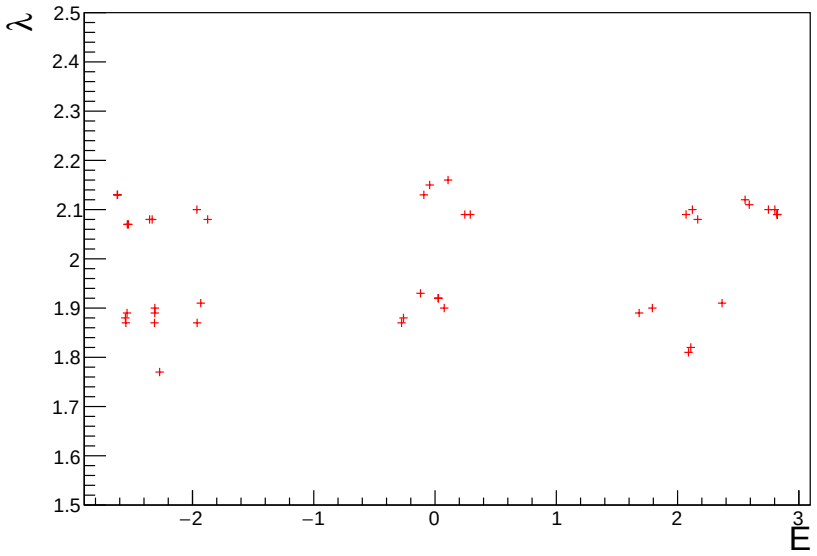

Figure 4.3: Plot of λ_c vs E_c for $t_2 = 0.1$. The points represent numerically determined λ_c and energy eigenvalues for different eigenstates for two open chains with 2000 lattice sites each other.

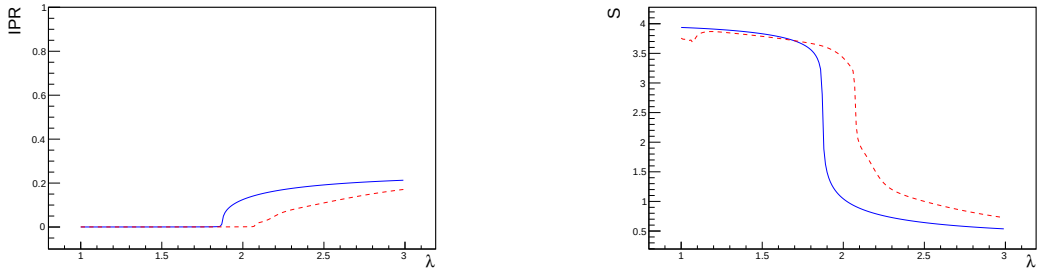

Figure 4.4: Shannon Entropy and the IPR as a function of the AA quasi-disorder potential strength λ for the ground state (blue line) and 499th excited state (red line) in a lattice with 2000 sites each other and $t_2 = 0.1$

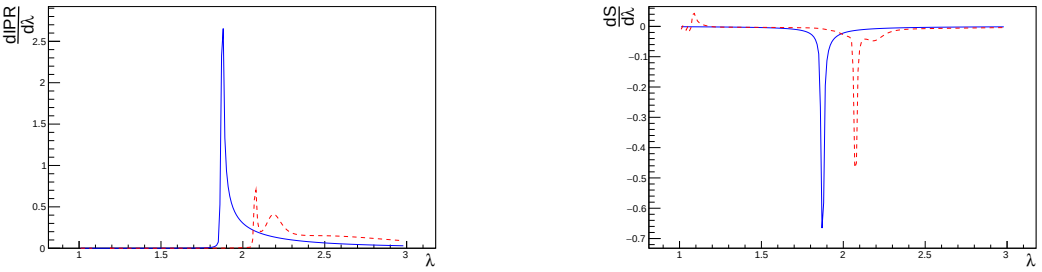

Figure 4.5: The variation of $\frac{dS}{d\lambda}$ and $\frac{dIPR}{d\lambda}$ with λ for the ground state (blue continue line) and 499th excited state (red dashed line) in a lattice with 2000 sites each other and $t_2 = 0.1$

4.2.2 Square Lattice

This system can be described by the Hamiltonian 4.2 where we assume $t_{2n,2n'} = t_{2n-1,2n'-1} = 1$, $t_{2n-1,2n} = t_d$ and $t_{2n-1,2n'} = 0 \quad \forall n \neq n'$:

$$\mathcal{H} = \sum_{n,j} \left(\hat{c}_n^\dagger \hat{c}_{n+j} + \hat{d}_n^\dagger \hat{d}_{n+j} \right) + t_d \sum_n \left(\hat{c}_n^\dagger \hat{d}_n + \hat{d}_n^\dagger \hat{c}_n \right) + \lambda \sum_n \cos(2\pi q n) \left(\hat{c}_n^\dagger \hat{c}_n + \hat{d}_n^\dagger \hat{d}_n \right)$$

Hence a particle can move only on nearest neighbors sites of same chain or on the site with the same energy that it start.
The eigenvalue equation is :

$$\mathcal{H}_n u_n = E u_n$$

In this case the matrix Hamiltonian is:

$$\mathcal{H}_n = \left[\begin{array}{c|c} M & t_2 \mathbb{1} \\ \hline t_2 \mathbb{1} & M \end{array} \right]$$

In figure 4.6 we have shown the variations of the S and IPR of the ground state as a function of the quasi-disorder strength for various values of t_d. The transition from the extended to the localized state is signaled by a large drop in S and a large rise in IPR.
In the absence of t_d the transition occurs at a critical disorder strength $\lambda_c = 2$, as we have seen in the first chapter. It is seen that λ_c doesn't change with t_d and no mobility edge appears (figures 4.7 and 4.8).

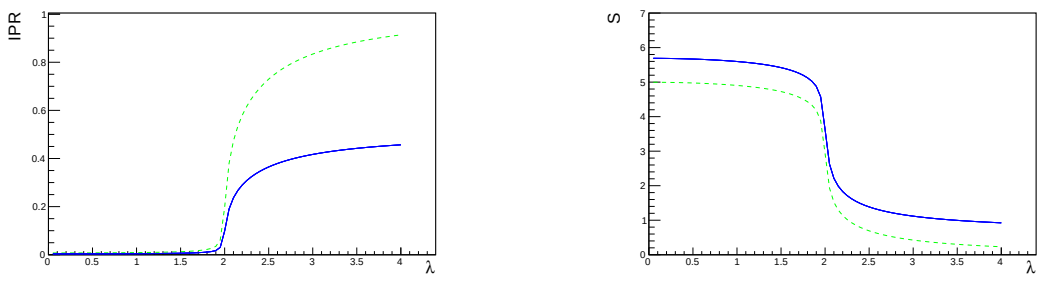

Figure 4.6: Shannon Entropy and the IPR as a function of the AA quasi-disorder potential strength λ for two open chains with 2000 lattice sites each other for different values of t_d . The green dashed line identify IPR and Shannon entropy curve for $t_d = 0$. We see that for $t_d \neq 0$ all curves are the same.

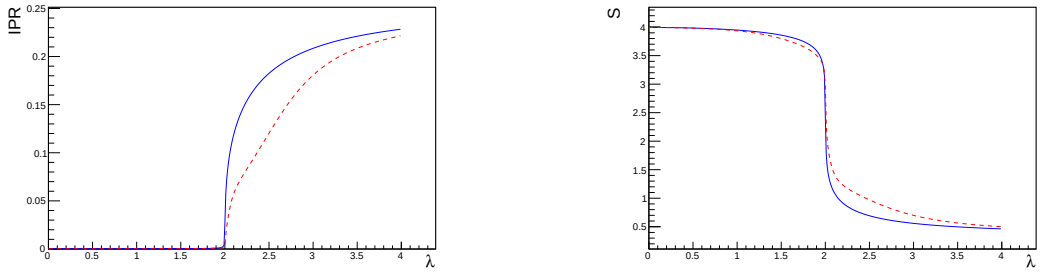

Figure 4.7: Shannon Entropy and the IPR as a function of the AA quasi-disorder potential strength λ for the ground state (blue continue line) and 200th excited state (red dashed line) in a lattice with 2000 sites each other and $t_2 = 0.1$.

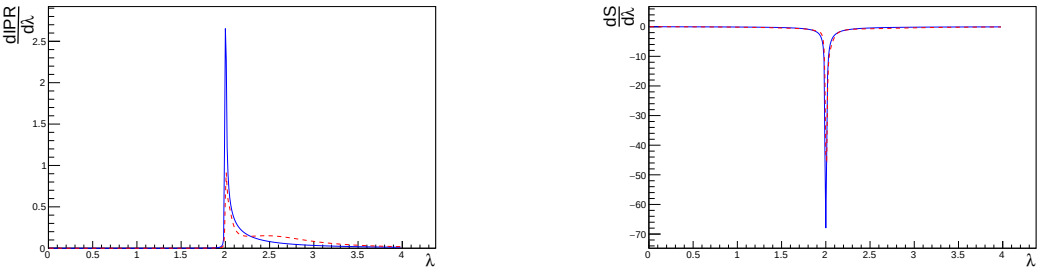

Figure 4.8: The variation of $\frac{dS}{d\lambda}$ and $\frac{dIPR}{d\lambda}$ with λ for the ground state (blue continue line) and 200th excited state (red dashed line) in a lattice with 2000 sites each other and $t_2 = 0.1$.

4.2.3 Square Lattice with energy shift

This system can be described by the Hamiltonian 4.2 where we assume $t_{2n,2n'} = t_{2n-1,2n'-1} = 1$, $t_{2n-1,2n} = t_d$, $t_{2n-1,2n'} = 0 \forall n \neq n'$ and different energy in situ:

$$\mathcal{H} = \sum_{n,j} \left(\hat{c}_n^\dagger \hat{c}_{n+j} + \hat{d}_n^\dagger \hat{d}_{n+j} \right) + t_d \sum_n \left(\hat{c}_n^\dagger \hat{d}_n + \hat{d}_n^\dagger \hat{c}_n \right) + \lambda \sum_n \left(\cos(2\pi q n) \hat{c}_n^\dagger \hat{c}_n + \cos(2\pi q (n+1)) \hat{d}_n^\dagger \hat{d}_n \right)$$

Hence a particle can move only on nearest neighbors sites of same chain or on the site with the same energy shifted by one that it start.
This Hamiltonian leads to the eigenvalue equation:

$$\mathcal{H}_n u_n = E u_n$$

In this case the matrix Hamiltonian is:

$$\mathcal{H}_n = \left[\begin{array}{c|c} M & t_2 \mathbb{1} \\ \hline t_2 \mathbb{1} & M' \end{array} \right]$$

where M' is:

$$M' = \begin{bmatrix} \epsilon_2 & 1 & 0 & \dots & 0 \\ 1 & \epsilon_3 & 1 & \ddots & \vdots \\ 0 & 1 & \epsilon_4 & \ddots & 0 \\ \vdots & \ddots & \ddots & \ddots & 1 \\ 0 & \dots & 0 & 1 & \epsilon_{n+1} \end{bmatrix}$$

In figure 4.9 and 4.10 we have shown the variations of the S and IPR of the ground state as a function of the quasi-disorder strength for various values of t_d. The transition from the extended to the localized state is signaled by a large drop in S and a large rise in IPR.
In the absence of t_d the transition occurs at a critical disorder strength $\lambda_c = 2$, as we have seen in chapter 1. It is seen that λ_c changes as t_d is introduced and the sign of t_d has a significant effect on the localization transition. The λ_c for the ground state increase with $|t_2|$ for $|t_2|$ and $t = 1$.
We have numerically obtained the λ_c for all the 4000 eigenstates from the calculations of the $\frac{dS}{d\lambda}$ as well as the $\frac{dIPR}{d\lambda}$ as a function of λ as shown in figure 3.4 for two states. We plotted in the figure 4.2.3 the variation of the λ_c for $t_d = 0.1$. The λ_c moves approximately inside two different values, which are the ground state critic strength and another λ_c approximately symmetric to the first with the axis $\lambda = 2$.

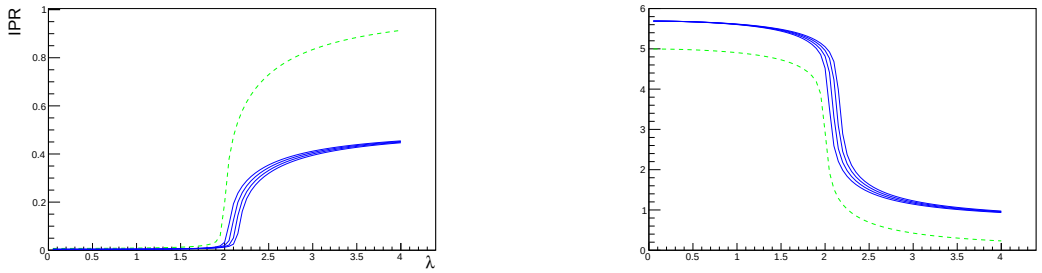

Figure 4.9: Shannon Entropy and the IPR as a function of the AA quasi-disorder potential strength λ for two open chains with 2000 lattice sites each other for different values of t_d . From left to right, the curves are for $t_d = -0.05$, -0.10, -0.15 , -0.20, respectively. The green dashed line identifies IPR and Shannon entropy curve for $t_d = 0$.

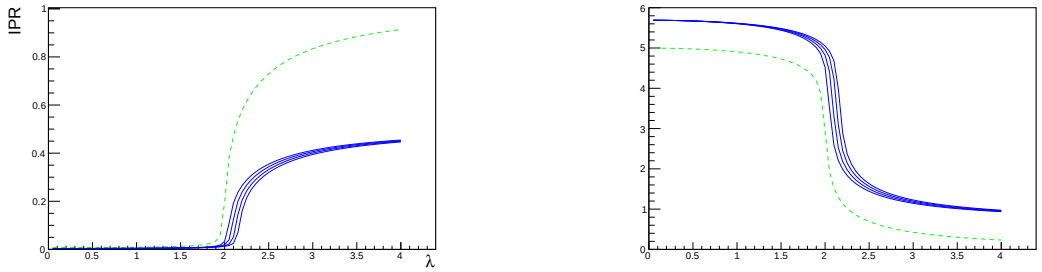

Figure 4.10: Shannon Entropy and the IPR as a function of the AA quasi-disorder potential strength λ for two open chains with 2000 lattice sites each other for different values of t_d . From left to right, the curves are for $t_d = 0.05$, 0.10, 0.15 , 0.20, respectively. The green dashed line identifies IPR and Shannon entropy curve for $t_d = 0$.

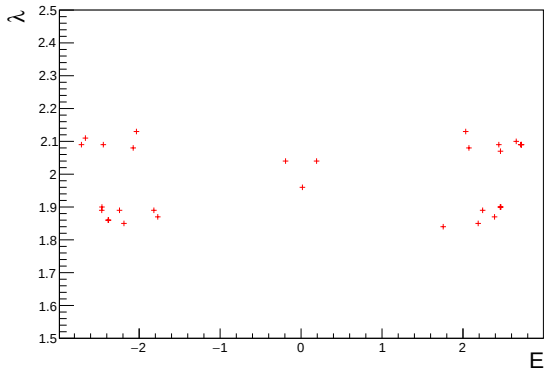

Figure 4.11: Plot of λ_c vs E_c for $t_2 = 0.1$. The points represent numerically determined λ_c and energy eigenvalues for different eigenstates for two open chains with 2000 lattice sites each other.

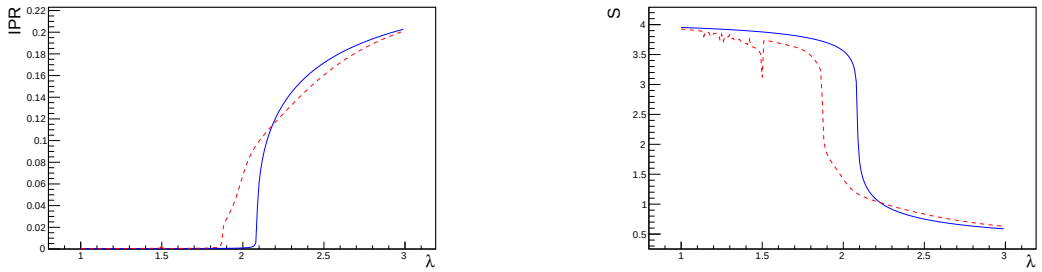

Figure 4.12: Shannon Entropy and the IPR as a function of the AA quasi-disorder potential strength λ for the ground state (blue continue line) and 499th excited state (red dashed line) in a lattice with 2000 sites each other and $t_2 = 0.1$.

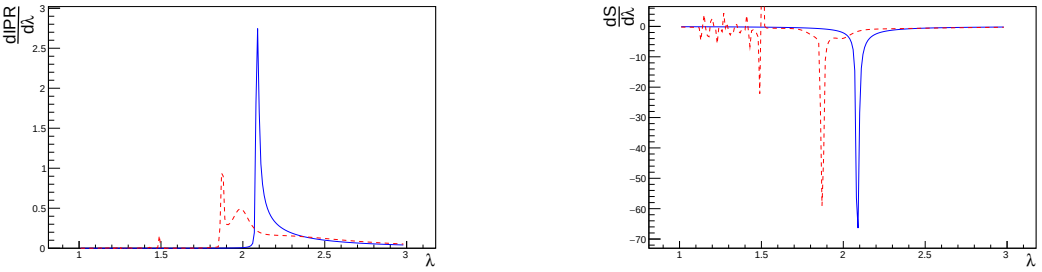

Figure 4.13: The variation of $\frac{dS}{d\lambda}$ and $\frac{dIPR}{d\lambda}$ with λ for the ground state (blue continue line) and 499th excited state (red dashed line) in a lattice with 2000 sites. each other and $t_2 = 0.1$.

Chapter 5

Analytical Calculations for quasi 1d systems

This chapter is devoted to analytical calculations in order to determine the value of λ_c on the localization transition for the configurations studied in the previous chapter. In the first and second section we present exact solution for the geometry structure of Square Lattice and Square Lattice with shift.
For the case of Triangular Lattice a discuss on the scheme of exact solution fails because it's not possible decouple the two chains. Hence we introduce the perturbation technique of Fröhlich transformation and study a more general case where the chains are quasi identical.

5.1 Exact Solution two chain as square lattice

Consider the following schematic view of two coupled chains as a square lattice:

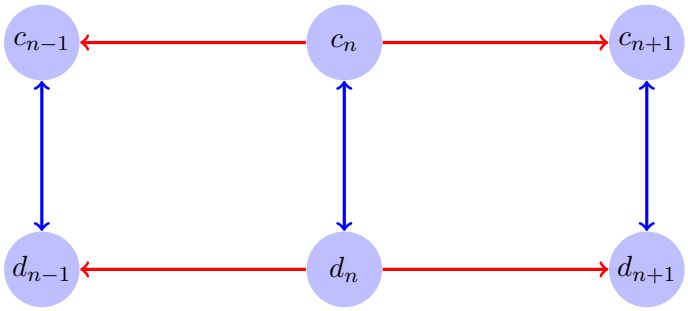

The Hamiltonian of this system is given by:

$$\mathcal{H} = \sum_n \epsilon(n)\hat{c}_n^\dagger \hat{c}_n + \sum_n \epsilon(n)\hat{d}_n^\dagger \hat{d}_n + t\sum_{n,j} \hat{c}_{n-j}^\dagger \hat{c}_n + t\sum_{n,j} \hat{d}_{n-j}^\dagger \hat{d}_n + t_d \sum_n \left(\hat{c}_n^\dagger \hat{d}_n + \hat{d}_n^\dagger \hat{c}_n\right)$$

It can be rewrite in terms of a spinor [23]:

$$\hat{b} := \begin{bmatrix} \hat{c} \\ \hat{d} \end{bmatrix}$$

$$\mathcal{H} = \sum_n \hat{b}_n^\dagger \bar{\bar{\epsilon}}(n) \hat{b}_n + t \sum_n \hat{b}_n^\dagger \mathbb{1} \hat{b}_{n+1} + t \sum_n \hat{b}_{n+1}^\dagger \mathbb{1} \hat{b}_n$$

where:

$$\bar{\bar{\epsilon}}(n) = \begin{bmatrix} \epsilon(n) & t_d \\ t_d & \epsilon(n) \end{bmatrix}$$

In the above, $\hat{c}$ and $\hat{d}$ are the annihilation operators at the nth site of the first and second chain, $\epsilon(n) = \lambda \cos(2\pi q n)$ is the on-site potential at the nth site of the both chain, t is the nearest neighbor hopping between the nth and the $(n+1)$th sites of every arm and t_d is the vertical hopping between the nth sites of the two chains.
We describe the system in a basis defined by the vector:

$$\mathbf{f}_n = \begin{bmatrix} f_{n,1} \\ f_{n,2} \end{bmatrix}$$

where $f_{n,j}$ is the amplitude of the wave function at the nth site of the jth chains ($j = 1, 2$).
So the Schroedinger equation in this basis, $\mathcal{H}\mathbf{f}_n = E\mathbf{f_n}$, leads to:

$$\left(E\mathbb{1} - \bar{\bar{\epsilon}}(n)\right) \mathbf{f}_n = t\mathbb{1} \left(\mathbf{f}_{n+1} + \mathbf{f}_{n-1}\right)$$

To determine the value of duality point we make the duality transformation define by $g_{m,j} = \sum_n e^{-i2\pi qnm} f_{n,j}$ for each arm of the ladder.
For the first ladder we've:

$$\sum_n \left[(E - \lambda \cos(2\pi q n)) f_{n,1} - t_d f_{n,2}\right] e^{-i2\pi qn} = t \sum_n (f_{n+1,1} + f_{n-1,1}) e^{-i2\pi qn}$$

that leads to:

$$(E - 2t\cos(2\pi qm)) gm, 1 - t_d g_{m,2} = \frac{\lambda}{2}(g_{m+1,1} + g_{m-1,1})$$

In the same way for the second chain we obtain:

$$(E - 2t\cos(2\pi qm)) gm, 2 - t_d g_{m,1} = \frac{\lambda}{2}(g_{m+1,2} + g_{m-1,2})$$

In a compact notation we can unify these two equations as:

$$\left[(E - 2t\cos(2\pi qm))\,\mathbb{1} - t_d \sigma_1\right] \mathbf{g_m} = \frac{\lambda}{2}\left(\mathbf{g_{m+1}} + \mathbf{g_{m-1}}\right)$$

where

$$\sigma_1 = \begin{bmatrix} 0 & 1 \\ 1 & 0 \end{bmatrix}$$

is the Pauli matrix.
We now diagonalize the σ_1 matrix by the matrix transformation:

$$\bar{\bar{S}} = \begin{bmatrix} 1 & 1 \\ 1 & -1 \end{bmatrix}$$

with the eigenvalue $1, -1$. The new basis is define by $\phi_m = \overline{\overline{S}}\mathbf{g}_m$.
The difference equation is now decouple into:

$$\begin{cases} (E - 2t\cos(2\pi qm) - t_d)\phi_{m,1} & = \frac{\lambda}{2}(\phi_{m+1,1} + \phi_{m-1,1}) \\ (E - 2t\cos(2\pi qm) + t_d)\phi_{m,2} & = \frac{\lambda}{2}(\phi_{m+1,2} + \phi_{m-1,2}) \end{cases}$$

The two equations represents the Aubry-André model with $\lambda_c = 2t$, as numerical calculations suggest.

5.2 Exact Solution two chain as square lattice with Shift

Now we consider the case of square lattice with Shift.
The Hamiltonian of this system is given by:

$$\mathcal{H} = \sum_n \epsilon(n)\hat{c}_n^\dagger \hat{c}_n + \sum_n \epsilon(n+1)\hat{d}_n^\dagger \hat{d}_n + t\sum_{n,j} \hat{c}_{n-j}^\dagger \hat{c}_n + t\sum_{n,j} \hat{d}_{n-j}^\dagger \hat{d}_n + t_d \sum_n \left(\hat{c}_n^\dagger \hat{d}_n + \hat{d}_n^\dagger \hat{c}_n\right)$$

It can be rewrite in terms of a spinor:

$$\hat{b} \coloneqq \begin{bmatrix} \hat{c} \\ \hat{d} \end{bmatrix}$$

$$\mathcal{H} = \sum_n \hat{b}_n^\dagger \overline{\overline{\epsilon}}(n)\hat{b}_n + t\sum_n \hat{b}_n^\dagger \mathbb{1}\hat{b}_{n+1} + t\sum_n \hat{b}_{n+1}^\dagger \mathbb{1}\hat{b}_n$$

where:

$$\overline{\overline{\epsilon}}(n) = \begin{bmatrix} \epsilon(n) & t_d \\ t_d & \epsilon(n+1) \end{bmatrix}$$

In the above, $\hat{c}$ and $\hat{d}$ are the annihilation operators at the nth site of the first and second chain, $\epsilon(n) = \lambda\cos(2\pi qn)$ is the on-site potential at the nth site of the both chain, t is the nearest neighbor hopping between the nth and the $(n+1)$th sites of every arm and t_d is the vertical hopping between the nth sites of the two chains.
We describe the system in a basis defined by the vector:

$$\mathbf{f}_n = \begin{bmatrix} f_{n,1} \\ f_{n,2} \end{bmatrix}$$

where $f_{n,j}$ is the amplitude of the wave function at the nth site of the jth chains $(j = 1, 2)$.
So the Schroedinger equation in this basis, $\mathcal{H}\mathbf{f}_n = E\mathbf{f_n}$, leads to:

$$\left(E\mathbb{1} - \overline{\overline{\epsilon}}(n)\right)\mathbf{f}_n = t\mathbb{1}\left(\mathbf{f}_{n+1} + \mathbf{f}_{n-1}\right)$$

To determine the value of duality point we make the duality transformation define by $g_{m,1} = \sum_n e^{-i2\pi qnm} f_{n,1}$ for the first arm and $g_{m,2} = \sum_n e^{-i2\pi q(n+1)m} f_{n,2}$ for the second arm of the ladder.

For the first chain we've:

$$\sum_n \left[(E - \lambda\cos(2\pi qn))f_{n,1} - t_d f_{n,2}\right] e^{-i2\pi qn} = t\sum_n (f_{n+1,1} + f_{n-1,1})e^{-i2\pi qn}$$

that leads to:

$$(E - 2t\cos(2\pi qm))g_{m,1} - t_d e^{i2\pi qm} g_{m,2} = \frac{\lambda}{2}(g_{m+1,1} + g_{m-1,1})$$

In the same way for the second chain we obtain:

$$(E - 2t\cos(2\pi q(m+1)))g_{m,2} - t_d e^{-i2\pi qm} g_{m,1} = \frac{\lambda}{2}(g_{m+1,2} + g_{m-1,2})$$

The first and second arm equation can write in a compact formula as:

$$E\mathbb{1}\mathbf{g}_m - \overline{\overline{M}}\mathbf{g}_m = \frac{\lambda}{2}(\mathbf{g}_{m+1} - \mathbf{g}_{m-1})$$

where we define the matrix:

$$\overline{\overline{M}} = \begin{bmatrix} 2t\cos(2\pi qm) & t_d e^{i2\pi qm} \\ t_d e^{-i2\pi qm} & 2t\cos(2\pi q(m+1)) \end{bmatrix}$$

In order to decouple the chains we must diagonalize $\overline{\overline{M}}$ matrix.
The characteristic polynomial is:

$$\begin{aligned} P(r) &= \det\overline{\overline{M}} - r\mathbb{1} = \left[2t\cos(2\pi qm) - r\right]\left[2t\cos(2\pi q(m+1)) - r\right] - t_d^2 \\ &= r^2 - 2tr(\cos(2\pi qm) + \cos(2\pi q(m+1))) + 4t^2\cos(2\pi qm)\cos(2\pi q(m+1)) - t_d^2 \end{aligned}$$

The condition $P(r) = 0$ leads to two solutions:

$$r_{1,2} = t\left(\cos(2\pi qm) + \cos(2\pi q(m+1))\right) \pm \sqrt{t_d^2 + t^2\left[\cos(2\pi qm) - \cos(2\pi q(m+1)\right]}$$

Now we consider the perturbation case where $t_d^2 \ll t^2\left[\cos(2\pi qm) - \cos(2\pi q(m+1)\right]$, so the eigenvalues becomes:

$$\begin{aligned} r_{1,2} &= t\left(\cos(2\pi qm) + \cos(2\pi q(m+1))\right) \\ &\pm t\left|\cos(2\pi qm) - \cos(2\pi q(m+1)\right| \sqrt{1 + \frac{t_d^2}{t^2\left[\cos(2\pi qm) - \cos(2\pi q(m+1)\right]}} \\ &\simeq t\left(\cos(2\pi qm) + \cos(2\pi q(m+1))\right) \pm t\left|\cos(2\pi qm) - \cos(2\pi q(m+1)\right| \\ &\frac{1}{2}\frac{t_d^2}{t\left|\cos(2\pi qm) - \cos(2\pi q(m+1))\right|} \end{aligned}$$

Now we've two different cases determine by the sign of $\cos(2\pi qm) - \cos(2\pi q(m+1))$:

1. $\operatorname{sgn}\left(\cos(2\pi qm) - \cos(2\pi q(m+1))\right) = 1$

$$r_1 = 2t\cos(2\pi qm) + \frac{1}{2t}\frac{t_d^2}{\cos(2\pi qm) - \cos(2\pi q(m+1))}$$
$$r_2 = 2t\cos(2\pi q(m+1)) - \frac{1}{2t}\frac{t_d^2}{t\cos(2\pi qm) - \cos(2\pi q(m+1))}$$

2. $\operatorname{sgn}(\cos(2\pi qm) + \cos(2\pi q(m+1))) = -1$

$$r_1 = 2t\cos(2\pi q(m+1)) - \frac{1}{2t}\frac{t_d^2}{\cos(2\pi qm) - \cos(2\pi q(m+1))}$$
$$r_2 = 2t\cos(2\pi qm) + \frac{1}{2t}\frac{t_d^2}{\cos(2\pi qm) - \cos(2\pi q(m+1))}$$

which present the same eigenvalues and this choice doesn't modify Schroedinger equations. After define the new vector basis $\phi_m = \overline{\overline{S'}}\mathbf{g}_m$, we obtain:

$$\begin{cases} \left[E - 2t\cos(2\pi qm) - \frac{1}{2t}\frac{t_d^2}{\cos(2\pi qm) - \cos(2\pi q(m+1))}\right]\phi_{m,1} & = \frac{\lambda}{2}(\phi_{m+1,1} + \phi_{m-1,1}) \\ \left[E - 2t\cos(2\pi q(m+1)) + \frac{1}{2t}\frac{t_d^2}{\cos(2\pi qm) - \cos(2\pi q(m+1))}\right]\phi_{m,2} & = \frac{\lambda}{2}(\phi_{m+1,2} + \phi_{m-1,2}) \end{cases}$$

For Schroedinger equations in real space we can apply the same procedure to decouple the ladder. In this case the eigenvalues are:

$$r_1 = \lambda\cos(2\pi qm) - \frac{t_d^2}{\lambda\cos(2\pi qm) - \lambda\cos(2\pi q(m+1))}$$
$$r_2 = \lambda\cos(2\pi q(m+1)) + \frac{t_d^2}{\lambda\cos(2\pi qm) - \lambda\cos(2\pi q(m+1))}$$

After we have defined new vector basis $\varphi_m = \overline{\overline{S''}}\mathbf{f}_m$, we obtain:

$$\begin{cases} \left(E - \epsilon(n) - \frac{t_d^2}{\epsilon(n) - \epsilon(n+1)}\right)\varphi_{m,1} & = t(\varphi_{m+1,1} + \varphi_{m-1,1}) \\ \left(E - \epsilon(n+1) - \frac{t_d^2}{\epsilon(n+1) - \epsilon(n)}\right)\varphi_{m,2} & = t(\varphi_{m+1,2} + \varphi_{m-1,2}) \end{cases}$$

This result matches with perturbation Hamiltonian description (see subsection 5.3.1). Analytically we have obtained the dual point at $\lambda = 2t$. Meanwhile numerically we have found a dependence of λ_c with the t_d hopping, in particular for the ground state.

5.3 Triangular and Square lattice formed by quasi-identical chains

In order to discuss the triangular lattice geometry we introduce a canonical transformation in a perturbation theory that sees the two chains as weakly coupled.
Consider the following schematic view of two coupled chains as a triangular lattice:

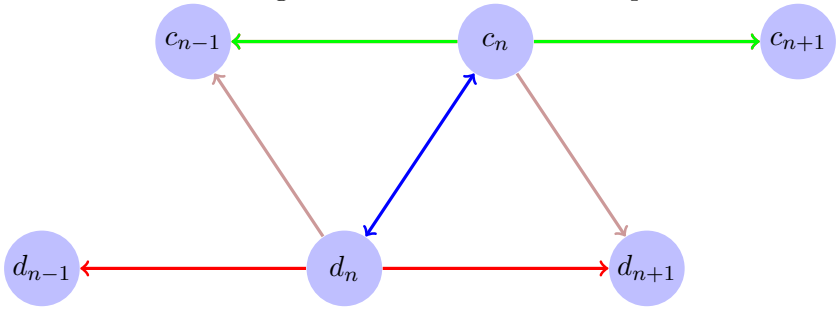

describes by the Hamiltonian:

$$\mathcal{H} = \sum_n \epsilon(n)\hat{c}_n^\dagger \hat{c}_n + \sum_n \epsilon(n+s)\hat{d}_n^\dagger \hat{d}_n + t_1 \sum_{n,j} \hat{c}_{n-j}^\dagger \hat{c}_n + t_2 \sum_{n,j} \hat{d}_{n-j}^\dagger \hat{d}_n + t_{ds} \sum_n \left(\hat{d}_n^\dagger \hat{c}_n + \hat{c}_n^\dagger \hat{d}_n\right) + t_d \sum_n \left(\hat{d}_{n+1}^\dagger \hat{c}_n + \hat{c}_{n-1}^\dagger \hat{d}_n\right) \tag{5.1}$$

In the above, $\hat{c}$ and $\hat{d}$ are the annihilation operators at the nth site of the first and second chain, $j = \pm 1$ is the locator of a nearest-neighbor site, $\epsilon(n) = \lambda \cos(2\pi q n)$ is the on-site potential at the nth site, s is the number of shifted sites ,t_1 is the nearest neighbor hopping between the nth and the $(n+1)$th sites of the first chain, t_2 is the nearest neighbor hopping between the nth and the $(n+1)$th sites of the second chain, t_{ds} is the vertical hopping between the nth sites of the two chains and t_d is the vertical hopping between the $n-1$ site of the first chain a n site of the second chain. Now we think about two weak coupled chains identified by a free Hamiltonian $\mathcal{H}_0$ and a perturbation Hamiltonian $\mathcal{H}_1$:

$$\begin{cases} \mathcal{H}_0 = \lambda \sum_n \cos(2\pi q n)\hat{c}_n^\dagger \hat{c}_n + \lambda \sum_n \cos(2\pi q(n+s))\hat{d}_n^\dagger \hat{d}_n + t_1 \sum_{n,j} \hat{c}_{n-j}^\dagger \hat{c}_n + t_2 \sum_{n,j} \hat{d}_{n-j}^\dagger \hat{d}_n + \\ \mathcal{H}_1 = t_{ds} \sum_n \left(\hat{d}_n^\dagger \hat{c}_n + \hat{c}_n^\dagger \hat{d}_n\right) + t_d \sum_n \left(\hat{d}_{n+1}^\dagger \hat{c}_n + \hat{c}_{n-1}^\dagger \hat{d}_n\right) \end{cases}$$

In this scheme we can use Fröhlich's approach Appendix C, to obtain a new Hamiltonian defined by:

$$\tilde{\mathcal{H}} = \mathcal{H}_0 + \frac{1}{2}[\mathcal{H}_1, S]$$

where $\hat{S}$ is an anti-Hermitian operator that satisfies the following constraint:

$$\mathcal{H}_1 + \left[\mathcal{H}_0, \hat{S}\right] = 0 \tag{5.2}$$

In this case we use the anti-Hermitian operator $\hat{S}$:

$$\hat{S} = \sum_m x_1(m)\hat{c}_m^\dagger \hat{d}_m + x_2(m)\hat{d}_m^\dagger \hat{c}_m - x_1^*(m)\hat{d}_m^\dagger \hat{c}_m - x_2^*(m)\hat{c}_m^\dagger \hat{d}_m \quad = \sum_m x(m)\hat{c}_m^\dagger \hat{d}_m - x^*(m)\hat{d}_m^\dagger \hat{c}_m$$

We calculate the commutator between the non-interacting Hamiltonian $\mathcal{H}_0$ and the operator $\hat{S}$.

$$\begin{aligned}\left[\mathcal{H}_0, \hat{S}\right] = &\sum_{m,n} \epsilon_1(n)x(m)\left[\hat{c}_n^\dagger \hat{c}_n, \hat{c}_m^\dagger \hat{d}_m\right] - \epsilon_1(n)x^*(m)\left[\hat{c}_n^\dagger \hat{c}_n, \hat{d}_m^\dagger \hat{c}_m\right] + \\ &\sum_{m,n} \epsilon_2(n)x(m)\left[\hat{d}_n^\dagger \hat{d}_n, \hat{c}_m^\dagger \hat{d}_m\right] - \epsilon_2(n)x^*(m)\left[\hat{d}_n^\dagger \hat{d}_n, \hat{d}_m^\dagger \hat{c}_m\right] + \\ &\sum_{m,n,j} t_1 x(m)\left[\hat{c}_{n-j}^\dagger \hat{c}_n, \hat{c}_m^\dagger \hat{d}_m\right] - t_1 x^*(m)\left[\hat{c}_{n-j}^\dagger \hat{c}_n, \hat{d}_m^\dagger \hat{c}_m\right] + \\ &\sum_{m,n,j} t_2 x(m)\left[\hat{d}_{n-j}^\dagger \hat{d}_n, \hat{c}_m^\dagger \hat{d}_m\right] - t_2 x^*(m)\left[\hat{d}_{n-j}^\dagger \hat{d}_n, \hat{d}_m^\dagger \hat{c}_m\right]\end{aligned}$$

Using the results reported in Appendix A we get

$$\begin{aligned}\left[\mathcal{H}_0, \hat{S}\right] = &\sum_{m,n} \epsilon_1(n)x(m)\delta_{n,m}\hat{c}_n^\dagger \hat{d}_m - \epsilon_1(n)x^*(m)(-\delta_{n,m})\hat{d}_m^\dagger \hat{c}_n + \\ &\sum_{m,n} \epsilon_2(n)x(m)(-\delta_{n,m})\hat{c}_m^\dagger \hat{d}_n - \epsilon_2(n)x^*(m)\delta_{n,m}\hat{d}_n^\dagger \hat{c}_m \\ &\sum_{m,n,j} t_1 x(m)\delta_{n,m}\hat{c}_{n-j}^\dagger \hat{d}_m - t_1 x^*(m)(-\delta_{n-j,m})\hat{d}_m^\dagger \hat{c}_n + \\ &\sum_{m,n,j} t_2 x(m)(-\delta_{n-j,m})\hat{c}_m^\dagger \hat{d}_n - t_2 x^*(m)\delta_{n,m}\hat{d}_{n-j}^\dagger \hat{c}_m \\ &= \sum_n \epsilon_1(n)x(n)\hat{c}_n^\dagger \hat{d}_n + \epsilon_1(n)x^*(n)\hat{d}_n^\dagger \hat{c}_n - \epsilon_2(n)x(n)\hat{c}_n^\dagger \hat{d}_n - \epsilon_2(n)x^*(n)\hat{d}_n^\dagger \hat{c}_n \\ &\sum_{n,j} t_1 x(n)\hat{c}_{n-j}^\dagger \hat{d}_n + t_1 x^*(n-j)\hat{d}_{n-j}^\dagger \hat{c}_n - t_2 x(n-j)\hat{c}_{n-j}^\dagger \hat{d}_n - t_2 x^*(n)\hat{d}_{n-j}^\dagger \hat{c}_n\end{aligned}$$

From the constraint 5.2 we obtain a set of six equations which determine the unknown $x(m)$.

$$\begin{cases} \hat{c}_n^\dagger \hat{d}_n \left(\epsilon_1(n)x(n) - \epsilon_2(n)x(n) + t_{ds}\right) = 0 & (5.3) \\ \hat{d}_n^\dagger \hat{c}_n \left(\epsilon_1(n)x^*(n) - \epsilon_2(n)x^*(n) + t_{ds}\right) = 0 & (5.4) \\ \hat{c}_{n+1}^\dagger \hat{d}_n \left(t_1 x(n) - t_2 x(n+1)\right) = 0 & (5.5) \\ \hat{c}_{n-1}^\dagger \hat{d}_n \left(t_1 x(n) - t_2 x(n-1) + t_d\right) = 0 & (5.6) \\ \hat{d}_{n+1}^\dagger \hat{d}_n \left(t_1 x^*(n+1) - t_2 x^*(n) + t_d\right) = 0 & (5.7) \\ \hat{d}_{n-1}^\dagger \hat{d}_n \left(t_1 x^*(n-1) - t_2 x^*(n)\right) = 0 & (5.8) \end{cases}$$

The equations 5.3 and 5.4 impose $x(n)$ must be real and in particular equal to:

$$x(n) = -\frac{t_{ds}}{\epsilon_1(n) - \epsilon_2(n)} \tag{5.9}$$

The other four equations must be consistent with 5.9. They can be separate into two different systems:

$$\begin{cases} t_1 x(n) - t_2 x(n+1) = 0 & (5.10) \\ t_1 x(n+1) - t_2 x(n) + t_d = 0 & (5.11) \end{cases}$$

$$\begin{cases} t_1 x(n) - t_2 x(n-1) + t_d = 0 & (5.12) \\ t_1 x(n-1) - t_2 x(n) = 0 & (5.13) \end{cases}$$

They leads the following solutions:

$$x(n) = \frac{t_d}{t_2} \frac{1}{1 - \left(\frac{t_1}{t_2}\right)^2} \tag{5.14}$$

$$x(n) = -\frac{t_d}{t_1} \frac{1}{1 - \left(\frac{t_2}{t_1}\right)^2} \tag{5.15}$$

The solutions are consistent when they live in accordance with the curve:

$$\frac{t_1^3 + t_2^3 - 2t_1 t_2}{t_1 t_2} = 0 \tag{5.16}$$

with the constraint $|t_1| \neq |t_2|$.

5.3.1 Square Lattice with shift

We return to consider the case of Square Lattice with shifted chains. To obtain this configuration we must set $t_d = 0$ into equations 5.6 and 5.7 .
In order to have consistency between the systems we must put $t_1 = t_2 := t_s$. Now we can calculate the commutator between $\mathcal{H}_1$ and $\hat{S}$.

$$\begin{aligned} \left[\mathcal{H}_1, \hat{S}\right] &= \sum_{m,n} \frac{t_{ds}^2}{\epsilon_1(m) - \epsilon_2(m)} \left[\hat{c}_n^\dagger \hat{d}_n + \hat{d}_n^\dagger \hat{c}_n, \hat{d}_m^\dagger \hat{c}_m - \hat{c}_m^\dagger \hat{d}_m\right] \\ &= \sum_{m,n} \frac{t_{ds}^2}{\epsilon_1(m) - \epsilon_2(m)} \left(\delta_{n,m} \hat{c}_n^\dagger \hat{c}_m - \delta_{n,m} \hat{d}_m^\dagger \hat{d}_n - \delta_{n,m} \hat{d}_n^\dagger \hat{d}_m + \delta_{n,m} \hat{c}_m^\dagger \hat{c}_n\right) \\ &= 2 \sum_n \frac{t_{ds}^2}{\epsilon_1(n) - \epsilon_2(n)} \left(\hat{c}_n^\dagger \hat{c}_n - \hat{d}_n^\dagger \hat{d}_n\right) \end{aligned}$$

The effective Hamiltonian becomes:

$$\begin{aligned} \tilde{\mathcal{H}} &= \mathcal{H}_0 + \frac{1}{2}\left[\mathcal{H}_1, S\right] \\ &= \sum_n \left(\epsilon_1(n) + \frac{t_{ds}^2}{\epsilon_1(n) - \epsilon_2(n)}\right) \hat{c}_n^\dagger \hat{c}_n + \sum_n \left(\epsilon_2(n) - \frac{t_{ds}^2}{\epsilon_1(n) - \epsilon_2(n)}\right) \hat{d}_n^\dagger \hat{d}_n + t_s \sum_{n,j} \left(\hat{c}_{n-j}^\dagger \hat{c}_n + \hat{d}_{n-j}^\dagger \hat{d}_n\right) \end{aligned} \tag{5.17}$$

The new Hamiltonian describes two decoupled chains similar to the Aubry-André model with a new energy in situ given by $\frac{t_{ds}^2}{\epsilon_1(n) - \epsilon_2(n)}$. This new model presents invariance by $t_{ds} \mapsto -t_{ds}$ in accordance with numerical results.

5.3.2 Triangular Lattice

We return to the case of Triangular Lattice. The hopping terms t_1 and t_2 must satisfy the equations 5.16 shown in figure 5.1. Now we must compare the equation 5.9 with 5.14 or 5.15:

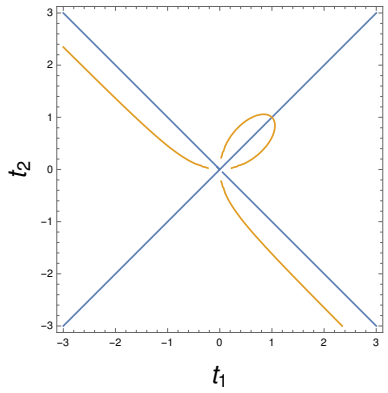

Figure 5.1: Hopping terms graph (orange line) in accordance with the curve 5.16.

$$\frac{t_{ds}}{\epsilon_1(n) - \epsilon_2(n)} = \frac{t_d}{t_1} \frac{1}{1 - \left(\frac{t_2}{t_1}\right)^2}$$

Hence we obtain:

$$\Delta := \epsilon_1(n) - \epsilon_2(n) = \frac{t_{ds}}{t_d}\left(t_1 - \frac{t_2^2}{t_1}\right) \tag{5.18}$$

In this case the energy in situ of the first chain must be equal to the energy in situ of the second chain plus a gap Δ.
In this perspective we obtain the unknown:

$$x = -\frac{t_{ds}}{\Delta}$$

Now we can calculate the commutator between $\mathcal{H}_1$ and $\hat{S}$.

$$\begin{aligned}
\left[\mathcal{H}_1, \hat{S}\right] &= \frac{t_{ds}}{\Delta} \sum_{m,n} \left[t_{ds}\hat{c}_n^\dagger \hat{d}_n + t_{ds}\hat{d}_n^\dagger \hat{c}_n + t_d \hat{c}_{n-1}^\dagger \hat{d}_n + t_d \hat{d}_{n+1}^\dagger \hat{c}_n, \hat{d}_m^\dagger \hat{c}_m - \hat{c}_m^\dagger \hat{d}_m\right] \\
&= \frac{t_{ds}}{\Delta} \sum_{m,n} t_{ds}\left[\hat{c}_n^\dagger \hat{d}_n + \hat{d}_n^\dagger \hat{c}_n, \hat{d}_m^\dagger \hat{c}_m - \hat{c}_m^\dagger \hat{d}_m\right] + t_d\left[\hat{c}_{n-1}^\dagger \hat{d}_n + \hat{d}_{n+1}^\dagger \hat{c}_n, \hat{d}_m^\dagger \hat{c}_m - \hat{c}_m^\dagger \hat{d}_m\right] \\
&= \frac{t_{ds}}{\Delta} \sum_{m,n} \left[2t_{ds}\delta_{m,n}\left(\hat{c}_n^\dagger \hat{c}_m - \hat{d}_m^\dagger \hat{d}_n\right) + t_d\left(\delta_{n,m}\hat{c}_{n-1}^\dagger \hat{c}_m - \delta_{n-1,m}\hat{d}_m^\dagger \hat{d}_n - \delta_{n,m}\hat{d}_{n+1}^\dagger \hat{d}_m + \delta_{n+1,m}\hat{c}_m^\dagger \hat{c}_n\right)\right] \\
&= \frac{2t_{ds}^2}{\Delta} \sum_n \left(\hat{c}_n^\dagger \hat{c}_n - \hat{d}_n^\dagger \hat{d}_n\right) + \frac{t_{ds}t_d}{\Delta} \sum_n \left(\hat{c}_{n-1}^\dagger \hat{c}_n + \hat{c}_{n+1}^\dagger \hat{c}_n - \hat{d}_{n-1}^\dagger \hat{d}_n - \hat{d}_{n+1}^\dagger \hat{d}_n\right)
\end{aligned}$$

The effective Hamiltonian becomes:

$$\begin{aligned}\tilde{\mathcal{H}} &= \mathcal{H}_0 + \frac{1}{2}\left[\mathcal{H}_1, S\right] \\ &= \sum_n \left(\epsilon_1(n) + \Delta + \frac{t_{ds}^2}{\Delta}\right)\hat{c}_n^\dagger \hat{c}_n + \sum_n \left(\epsilon_1(n) - \frac{t_{ds}^2}{\Delta}\right)\hat{d}_n^\dagger \hat{d}_n \\ &+ \left(t_1 + \frac{t_{ds}t_d}{2\Delta}\right)\sum_{n,j}\hat{c}_{n-j}^\dagger \hat{c}_n + \left(t_2 - \frac{t_{ds}t_d}{2\Delta}\right)\sum_{n,j}\hat{d}_{n-j}^\dagger \hat{d}_n \end{aligned} \tag{5.19}$$

This new Hamiltonian describes two decoupled Aubry-André chains with the energy in situ difference by a constant and two different nearest neighbor hopping. The eigenvalue equations are:

$$\begin{cases} \left(\epsilon_1(n) + \Delta + \frac{t_{ds}^2}{\Delta}\right)u_n + \left(t_1 + \frac{t_{ds}t_d}{2\Delta}\right)(u_{n+1} + u_{n-1}) = Eu_n & (5.20) \\ \left(\epsilon_1(n) - \frac{t_{ds}^2}{\Delta}\right)u_n + \left(t_2 - \frac{t_{ds}t_d}{2\Delta}\right)(u_{n+1} + u_{n-1}) = Eu_n & (5.21) \end{cases}$$

This model implies the existence of two different strength critic parameter:

$$\lambda_{c,1} = 2t_1 + \frac{t_{ds}t_d}{\Delta} \tag{5.22}$$

$$\lambda_{c,2} = 2t_2 - \frac{t_{ds}t_d}{\Delta} \tag{5.23}$$

$$\tag{5.24}$$

This Hamiltonian is invariant by $t_{ds} \mapsto -t_{ds}$ and $t_d \mapsto -t_d$ respectively, like numerical calculations suggest. The ground state is described by the decoupled chain with lower energy. Hence the critical parameter is given by $\lambda_{c,1} = 2t_2 - \frac{t_{ds}t_d}{\Delta}$.

5.4 Square Lattice with shift in a new perspective

An equivalent description of Square Lattice with shift system is given by two identical chains with a transversal hopping between a site of the first chain with energy $\epsilon(n)$ and a site of the second chain with energy $\epsilon(n+1)$. This perspective leads to consider the Triangular Lattice Hamiltonian 5.1 and puts $t_{ds} = 0$, $s = 0$.
From the Hamiltonian:

$$\mathcal{H} = \sum_n \epsilon(n)\hat{c}_n^\dagger \hat{c}_n + \sum_n \epsilon(n)\hat{d}_n^\dagger \hat{d}_n + t_1 \sum_{n,j} \hat{c}_{n-j}^\dagger \hat{c}_n + t_2 \sum_{n,j} \hat{d}_{n-j}^\dagger \hat{d}_n + \\ + t_d \sum_n \left(\hat{d}_{n+1}^\dagger \hat{c}_n + \hat{c}_{n-1}^\dagger \hat{d}_n \right)$$

we apply the Fröhlich procedure in the same way as before. We obtain an anti-hermitian operator $\hat{S}$:

$$\hat{S} = -\frac{t_d}{t_1} \frac{1}{1 - \left(\frac{t_2}{t_1}\right)^2} \sum_m \left(\hat{c}_m^\dagger \hat{d}_m - \hat{d}_m^\dagger \hat{c}_m \right)$$

where the hopping terms t_1 and t_2 live in the curve described by 5.16.
Finally we obtain the effective Hamiltonian:

$$\begin{aligned} \tilde{\mathcal{H}} &= \mathcal{H}_0 + \frac{1}{2}[\mathcal{H}_1, S] \\ &= \sum_n \epsilon(n)\hat{c}_n^\dagger \hat{c}_n + \sum_n \epsilon(n)\hat{d}_n^\dagger \hat{d}_n \\ &+ \left(t_1 + \frac{t_d^2}{2t_1} \frac{1}{1 - \left(\frac{t_2}{t_1}\right)^2} \right) \sum_{n,j} \hat{c}_{n-j}^\dagger \hat{c}_n + \left(t_2 - \frac{t_d^2}{2t_1} \frac{1}{1 - \left(\frac{t_2}{t_1}\right)^2} \right) \sum_{n,j} \hat{d}_{n-j}^\dagger \hat{d}_n \end{aligned} \tag{5.25}$$

The Square Lattice with shift system is transformed into two Aubry-André chains with identical on-site energy $\epsilon(n)$.The eigenvalue equations are:

$$\begin{cases} \epsilon(n)u_n + T_1(u_{n+1} + u_{n-1}) = Eu_n & (5.26) \\ \epsilon(n)u_n + T_2(u_{n+1} + u_{n-1}) = Eu_n & (5.27) \end{cases}$$

where we defined $T_1 \coloneqq t_1 + \frac{t_d^2}{2t_1} \frac{1}{1-\left(\frac{t_2}{t_1}\right)^2}$ and $T_2 \coloneqq t_2 - \frac{t_d^2}{2t_1} \frac{1}{1-\left(\frac{t_2}{t_1}\right)^2}$. With this definitions $T_1 > T_2$. In order to find in which chains ground state belongs, we rescale both eigenvalue equations in units of T_1. Hence we obtain:

$$\begin{cases} \epsilon(n)' u_n + (u_{n+1} + u_{n-1}) = E' u_n \\ \epsilon(n)' u_n + \frac{T_2}{T_1}(u_{n+1} + u_{n-1}) = E' u_n \end{cases}$$

The critical values, in these units, are $\lambda_{c,1} = 2$ and $\lambda_{c,2} = 2\frac{T_2}{T_1} < 2$. As we observed, for example in chapter 1, the energy spectrum becomes much larger when the energy strength λ increases. So the ground state energy lives in the chain with greater λ_c that is described by 5.26.

Finally the law that describes the critical strength is:

$$\lambda_c = 2\left(t_1 + \frac{t_d^2}{2t_1}\frac{1}{1-\left(\frac{t_2}{t_1}\right)^2}\right) \tag{5.28}$$

In the particular case where $t_d = t_{ds}$, the triangular lattice and square lattice with shift show a similar behavior about localization transition. In fact the critical values 5.22 and 5.23 match with eigenvalue equations 5.26 and 5.27. The localization transition for the ground state of the first system is determined by

$$\lambda_{c,1} = 2t_1 + \frac{t_d^2}{\Delta} \tag{5.29}$$

whereas for the second system:

$$\lambda_{c,2} = 2t_2 - \frac{t_d^2}{\Delta} \tag{5.30}$$

The excited states for these systems are described in accordance with the energy spectrum of the eigenvalue equations 5.26 and 5.27 for the square lattice with shift and 5.20 and 5.21 for triangular lattice.

5.5 The value of Δ

This parameter is introduced in triangular lattice scheme in order to apply a perturbation Frolich's approach. A way to obtain the value of Δ is though the comparison between Frolich's approach and exact analytical calculation. In particular we study the model proposed by *Sil et al.* in [23] and discussed by *Flach* and *Danieli* in [24].
The hamiltonian of ladder network, using the notation introduced in section 5.1, is:

$$\mathcal{H} = \sum_n \hat{b}_n^\dagger \bar{\bar{\epsilon}}(n)\hat{b}_n + \sum_n \hat{b}_n^\dagger \bar{\bar{t}}\hat{b}_{n+1} + h.c.$$

where:

$$\bar{\bar{\epsilon}}(n) = \begin{bmatrix} \epsilon(n) & t_{ds} \\ t_{ds} & \epsilon(n) \end{bmatrix}$$

and

$$\bar{\bar{t}} = \begin{bmatrix} t_s & t_d \\ t_d & t_s \end{bmatrix}$$

The Schroedinger equation leads to:

$$(E\mathbb{1} - \bar{\bar{\epsilon}}(n))\,\mathbf{f}_n = \bar{\bar{t}}\,(\mathbf{f}_{n+1} + \mathbf{f}_{n-1}) \tag{5.31}$$

that reads also as:

$$\begin{cases} (E-\epsilon(n))f_{n,1} - t_{ds}f_{n,2} & = t_s(f_{n+1,1} + f_{n-1,1}) + t_d(f_{n+1,2} + f_{n-1,2}) \\ (E-\epsilon(n))f_{n,2} - t_{ds}f_{n,1} & = t_s(f_{n+1,2} + f_{n-1,2}) + t_d(f_{n+1,1} + f_{n-1,1}) \end{cases}$$

We rewrite this equations by transforming to $f_n^{\pm} = \frac{f_{n,1} \pm f_{n,2}}{\sqrt{2}}$. So we apply to both members of 5.31 the change basis matrix defined by:

$$P = \begin{bmatrix} \frac{\sqrt{2}}{2} & \frac{\sqrt{2}}{2} \\ \frac{\sqrt{2}}{2} & -\frac{\sqrt{2}}{2} \end{bmatrix}$$

Evaluating term by term we have:

$$P\bar{\bar{\epsilon}}(n)\mathbf{f_n} = \begin{bmatrix} (\epsilon(n) + t_{ds}) f_n^+ \\ (\epsilon(n) - t_{ds}) f_n^- \end{bmatrix}$$

and

$$P\bar{\bar{t}}\mathbf{f_n} = \begin{bmatrix} (t_s + t_d) f_n^+ \\ (t_s - t_d) f_n^- \end{bmatrix}$$

In this new basis is decoupled into two non-interacting chains described by the eigenvalue equations:

$$\begin{cases} [E - (\epsilon(n) + t_{ds})]\, f_n^+ & = (t_s + t_d)(f_{n+1}^+ + f_{n-1}^+) \\ [E - (\epsilon(n) - t_{ds})]\, f_n^+ & = (t_s - t_d)(f_{n+1}^- + f_{n-1}^-) \end{cases} \tag{5.32}$$

The problem detangles into two independent one-dimensional tight-binding chains with spectra $E^{\pm}$. All states of any of the two $f^{\pm}$ chains transit simultaneously at $\lambda_c^{\pm} = 2\,|t_s \pm t_d|$.
Now we see the same problem in a perturbation point of view.
We start from the Hamiltonian:

$$\mathcal{H} = \sum_{n,r} T_1(n,|r|)\hat{c}_n^{\dagger}\hat{c}_{n+r} + \sum_{n,r} T_2(n,|r|)\hat{d}_n^{\dagger}\hat{d}_{n+r} + \sum_{n,\omega} T_D(n,\omega)\hat{c}_n^{\dagger}\hat{d}_{n+\omega} + \sum_{n,\omega} T_D(n,\omega)\hat{d}_{n+\omega}^{\dagger}\hat{c}_n \tag{5.33}$$

where we define

$$T_1(n,|r|) = \begin{cases} \epsilon(n) + \Delta & if \quad r = 0 \\ t_1 & if \quad |r| = 1 \end{cases}$$

$$T_2(n,|r|) = \begin{cases} \epsilon(n) & if \quad r = 0 \\ t_2 & if \quad |r| = 1 \end{cases}$$

$$T_D(n,\omega) = \begin{cases} t_{ds} & if \quad \omega = 0 \\ t_d & if \quad |\omega| = 1 \end{cases}$$

We use the anti-Hermitian operator

$$\hat{S} = \sum_m x(m)\hat{c}_m^{\dagger}\hat{d}_m - x^*(m)\hat{d}_m^{\dagger}\hat{c}_m$$

In the same way as Triangular lattice the condition $\mathcal{H}_1 + \left[\mathcal{H}_0, \hat{S}\right] = 0$ leads to $x = -\frac{t_{ds}}{\Delta}$. The effective Hamiltonian comes immediately after explicated the commutator $\left[\mathcal{H}_1, \hat{S}\right]$:

$$\begin{aligned}
\left[\mathcal{H}_1, \hat{S}\right] &= \frac{t_{ds}}{\Delta} \sum_{m,n,\omega} T_D(\omega) \left[\hat{c}_n^\dagger \hat{d}_{n+\omega} + \hat{d}_{n+\omega}^\dagger \hat{c}_n, \hat{d}_m^\dagger \hat{c}_m - \hat{c}_m^\dagger \hat{d}_m\right] \\
&= \frac{t_{ds}}{\Delta} \sum_{m,n,\omega} T_D(\omega) \left(\left[\hat{c}_n^\dagger \hat{d}_{n+\omega}, \hat{d}_m^\dagger \hat{c}_m\right] - \left[\hat{c}_n^\dagger \hat{d}_{n+\omega}, \hat{c}_m^\dagger \hat{d}_m\right] + \left[\hat{d}_{n+\omega}^\dagger \hat{c}_n, \hat{d}_m^\dagger \hat{c}_m\right] - \left[\hat{d}_{n+\omega}^\dagger \hat{c}_n, \hat{c}_m^\dagger \hat{d}_m\right]\right) \\
&= 2\frac{t_{ds}}{\Delta} \sum_{m,n,\omega} T_D(\omega) \hat{c}_n^\dagger \hat{c}_m - 2\frac{t_{ds}}{\Delta} \sum_{m,n,\omega} T_D(\omega) \hat{c}_n^\dagger \hat{c}_m \\
&= \frac{2t_{ds}^2}{\Delta} \sum_n \left(\hat{c}_n^\dagger \hat{c}_n - \hat{d}_n^\dagger \hat{d}_n\right) + 2\frac{t_{ds} t_d}{\Delta} \sum_{n,\omega=\pm 1} \left(\hat{c}_n^\dagger \hat{c}_{n+\omega} - \hat{d}_n^\dagger \hat{d}_{n+\omega}\right)
\end{aligned}$$

Finally the effective Hamiltonian becomes:

$$\begin{aligned}
\tilde{\mathcal{H}} &= \mathcal{H}_0 + \frac{1}{2}\left[\mathcal{H}_1, S\right] \\
&= \sum_n \left(\epsilon_1(n) + \Delta + \frac{t_{ds}^2}{\Delta}\right) \hat{c}_n^\dagger \hat{c}_n + \sum_n \left(\epsilon_1(n) - \frac{t_{ds}^2}{\Delta}\right) \hat{d}_n^\dagger \hat{d}_n \\
&+ \left(t_1 + \frac{t_{ds} t_d}{\Delta}\right) \sum_{n,\omega=\pm 1} \hat{c}_{n+\omega}^\dagger \hat{c}_n + \left(t_2 - \frac{t_{ds} t_d}{\Delta}\right) \sum_{n,\omega=\pm 1} \hat{d}_{n+\omega}^\dagger \hat{d}_n
\end{aligned}$$

The strength critic parameters are :

$$\lambda_{c,1} = 2\left(t_1 + \frac{t_{ds} t_d}{\Delta}\right) \tag{5.34}$$

$$\lambda_{c,2} = 2\left(t_2 - \frac{t_{ds} t_d}{\Delta}\right) \tag{5.35}$$

$$\tag{5.36}$$

Comparing these results with 5.32 leads the equality $\Delta = t_{ds}$.

5.6 Phase Diagrams

Finally we can summarize the results found in this chapter in the phase diagrams. In the same way as chapter 1 and chapter 3 we have calculated the IPR-function for each energy of the system. After choosing a IPR-threshold defined by the value of λ where we have found numerically a localization transition, we have discriminated localized states from delocalized states based on the value of the eigenstates IPR-function. The numerical details are shown in table 5.1.

So if this value is greater than the threshold the state is localized, otherwise the state is delocalized. This procedure leads to the figures 5.2, 5.3 and 5.4.

System	λ_c	n eigenstate	Energy	IPR-threshold
Triangular Lattice	1.87	Ground state	-2.54929	0.0126886
Square Lattice with Shift	2.09	Ground state	-2.72165	0.0391663
Square Lattice with Shift (5.17)	2.09	3979	2.63933	0.1633

Table 5.1: Numerical details used to build the phases diagrams in figures 5.2, 5.3 and 5.4.

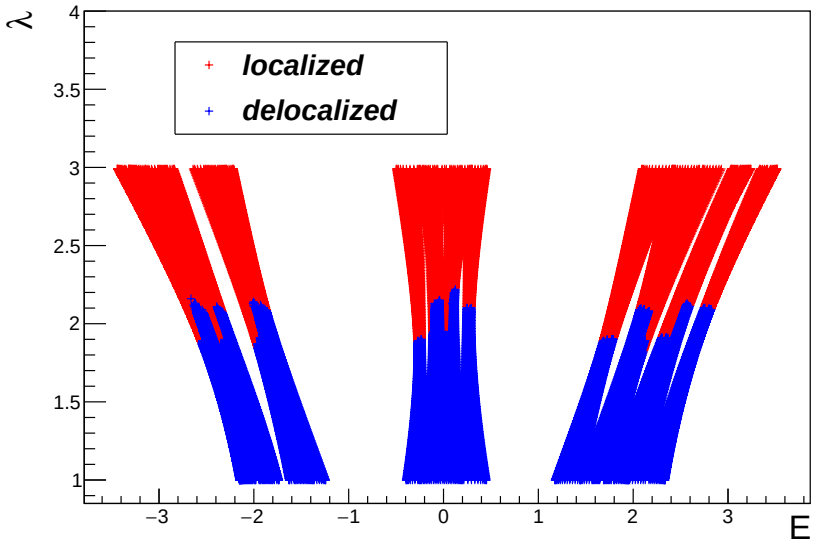

Figure 5.2: Phase Diagram triangular lattice for $t_d = 0.1$

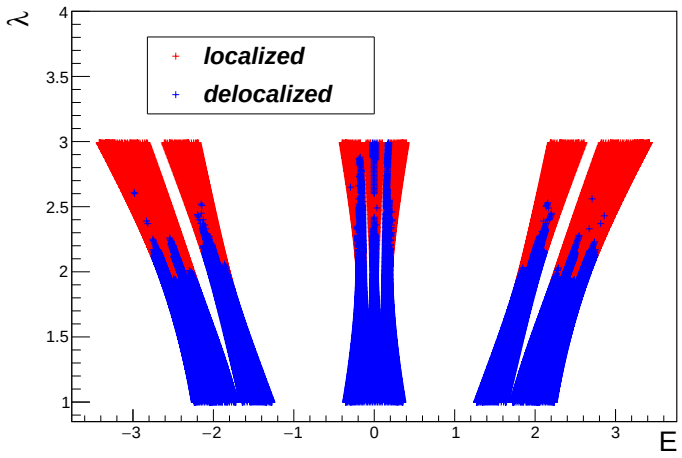

Figure 5.3: Phase Diagram square lattice with shift for $t_d = 0.1$

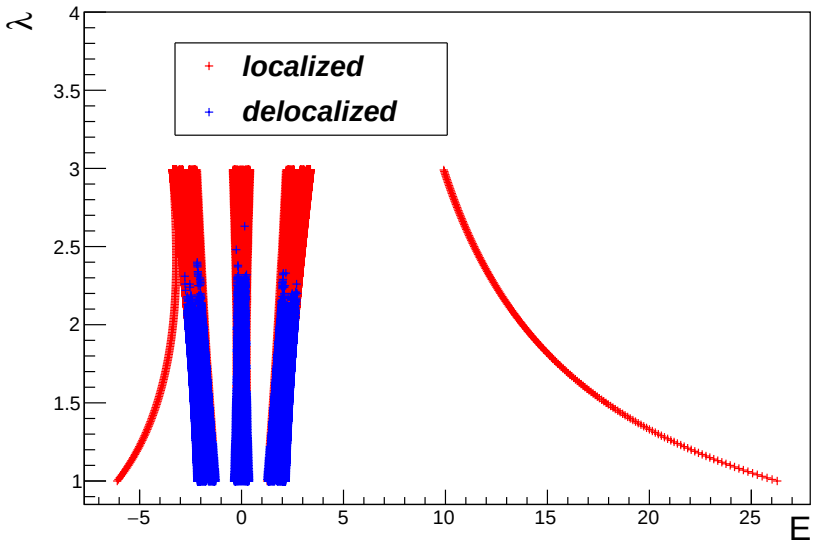

Figure 5.4: Phase Diagram square lattice with shift after Fröhlich transformation described by the Hamiltonian 5.17 for $t_d = 0.1$

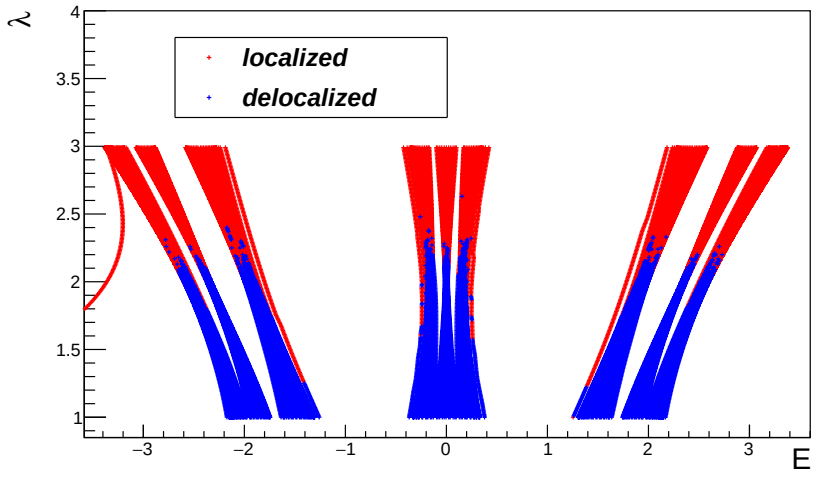

Figure 5.5: Zoom of figure 5.4

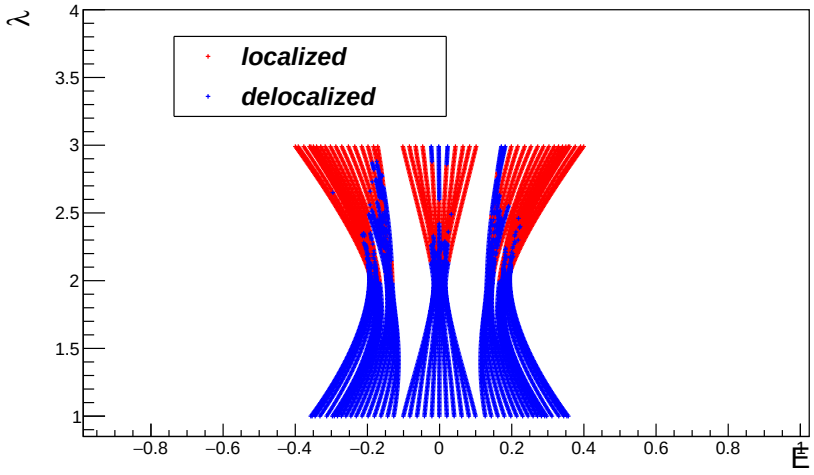

Figure 5.6: Zoom of figure 5.3 in the middle of energy spectrum

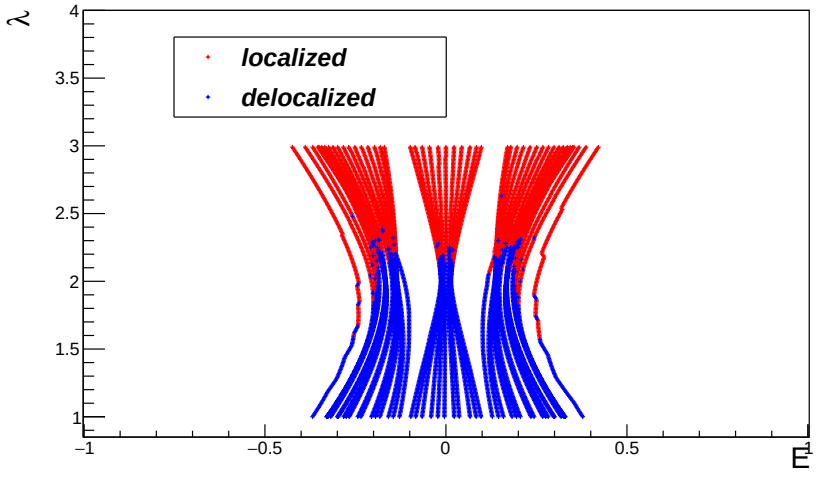

Figure 5.7: Zoom of figure 5.4 in the middle of energy spectrum

From the phase diagram of triangular lattice (figure 5.2) we see the two different strength critic parameters. The energy spectrum appears symmetric respect the λ axis. This suggest us that this system is an overlap of two different Aubry-André chains with different hopping terms.

Also from the phase diagram of Square with shift Lattice we can observe the two critic parameters on the left and right sides of the energy spectrum. In the middle the states appear almost everywhere delocalized. This effect probably comes from the shift between the two chains that becomes more relevant near $E \simeq 0$.
We note in figures 5.4, 5.5 and 5.7 that the Hamiltonian 5.17 could describe a possible mobility edge in the middle of the band, like we can observe in the phase diagram 5.6.
Otherwise the Hamiltonian 5.25 identifies the two critic parameters emphasized in the phase diagram 5.3.

In order to compare the results of numerical and analytical calculations, we consider the Hamiltonians 5.19 and 5.25 with the hopping terms $t_1 \simeq t_2 \simeq 1$. We expand them like:

$$\begin{cases} t_1 &= 1+\varepsilon \\ t_2 &= 1+\delta \end{cases} \tag{5.37}$$

with $(\varepsilon, \delta) \to (0,0)$.
The equation 5.16 becomes:

$$\begin{aligned} f(\varepsilon,\delta) &= (1+\varepsilon)^3 + (1+\delta)^3 - 2(1+\varepsilon)(1+\delta) \\ &\simeq 1 + 3\varepsilon + 3\varepsilon^2 + 1 + 3\delta + 3\delta^2 - 2 - 2\varepsilon - 2y - 2\varepsilon\delta \\ &\simeq 3\varepsilon^2 + 3\delta^2 + \varepsilon + \delta - 2\varepsilon\delta \end{aligned}$$

For Δ, expressed in equation 5.18, we have:

$$\begin{aligned} \Delta\frac{t_d}{t_{ds}} &\simeq \left[(1+\varepsilon)^2 - (1+\delta)^2\right](1-\varepsilon) \\ &\simeq -\varepsilon^2 - \delta^2 + 2\varepsilon - 2\delta + 2\varepsilon\delta \end{aligned}$$

ε and δ must satisfy the system:

$$\begin{cases} 3\varepsilon^2 + 3\delta^2 + \varepsilon + \delta - 2\varepsilon\delta = 0 \\ -\varepsilon^2 - \delta^2 + 2\varepsilon - 2\delta + 2\varepsilon\delta = \Delta\frac{t_d}{t_{ds}} \end{cases} \tag{5.38}$$

For numerical cases we used $t_{ds} = t_d = 0.05, 0.10, 0.15$. As we have seen in section 5.5, we put $\Delta = t_{ds}$ and solve numerically (with Mathematica) the system 5.38.
The stregth critic parameters, $\lambda_{c,gs}$ for the ground state and $\lambda_{c,ex}$ for an excited state, can now resume as:

$$\begin{cases} \lambda_{c,gs} = 2t_2 - t_d \\ \lambda_{c,ex} = 2t_1 + t_d \end{cases} \tag{5.39}$$

for triangular lattice and

$$\begin{cases} \lambda_{c,gs} = 2t_1 + t_d \\ \lambda_{c,ex} = 2t_2 - t_d \end{cases} \tag{5.40}$$

for Square lattice with shift. Finally we can propose the comparison between numerical and analytical calculations that determine the value of critic strength parameter λ_c in function of t_d, for triangular (figure 5.8) and square with shift (figure 5.9) lattices.

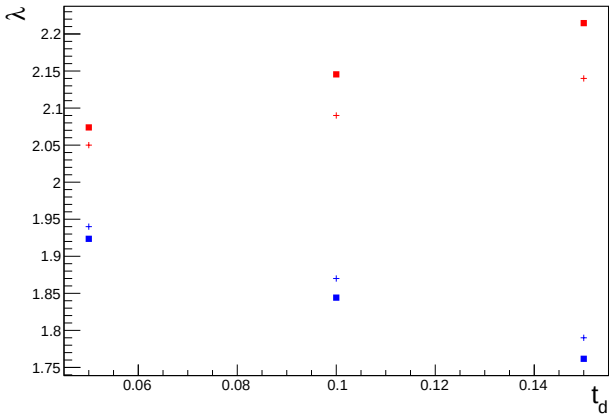

Figure 5.8: Triangular Lattice comparison between numerical (plus marker) and analytical (square marker) calculations (5.39) for ground state (blue marker) and excited state (red marker) energy

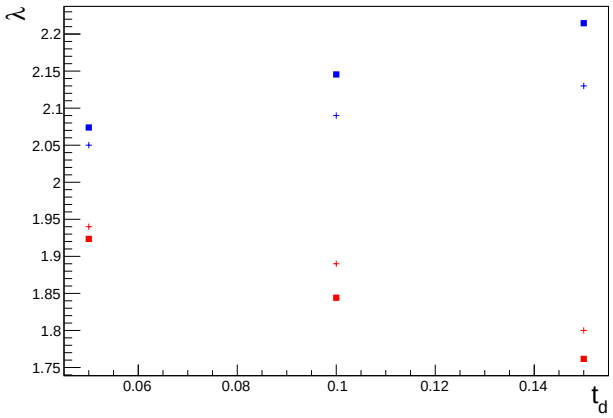

Figure 5.9: Square with shift Lattice comparison between numerical (plus marker) and analytical (square marker) calculations (5.40) for ground state (blue marker) and excited state (red marker) energy

Conclusions

We have reviewed some important properties of Aubry-André model, using IPR and Shannon entropy as tools to determine the localization transition.

From the strong relation between the Hofstader 2D model and the Harper model we have seen numerically the existence of almost localized states. This complex states do not conflict with the non-existence of a true mobility edge, which is a consequence of an exact self-duality of the model. However, if the incommensurate parameter $\tau \ll 1$, as we have seen with the inverse participation ratio (IPR) estimator, there are two "effective" mobility edges at the critical energies $E_c = \pm(2t - \lambda)$ for $\lambda < 2t$ [19], where λ and t are the strength potential parameter and the nearest-neighbor hopping respectively. Hence the states near the band edges are almost localized even for a weak incommensurate potential. This implies that the fractal dimension of the system, obtained though the correlation density function, is well defined only for $E \simeq 0$ and not for all E like *Zdetsis et al* in [20] suggested.

The mobility edge appears in 1D Aubry-André model when next nearest-neighbor hopping t_2 is included. In the ground state a negative t_2 enhances the critical disorder strength λ_c required for the localization transition, while a positive t_2 reduces λ_c. For the states with energy $E > 0$, the trend is opposite. These results are obtained numerically and analytically summarized by the formula [18]

$$\lambda_c = \frac{2t_1 + 2E\left(\frac{t_2}{t_1}\right)}{1 + \left(\frac{t_2}{t_1}\right)^2}$$

Hence the critical parameter λ_c depends almost linearly on t_2 at fixed value of E, and linearly on E at fix value of $t_2 \neq 0$.

The aim of this work is the study of two weakly coupled chains. We have verified, numerically and analytically, that no clear mobility edges appear in the geometry of triangular, square and square with shift lattice but there is a regime of parameters in the spectrum where extended and localized states coexist. In particular we have seen, with a change of basis, that square lattice geometry is equivalent to two decoupled Aubry-André chains with $\lambda_c = 2t$. Whereas for triangular and square lattice with shift it is not possible to apply an exact method to reduce the system to a simple one. Hence we decided to adopt a perturbation theory in order to decrease the degrees of freedom. Using the time-independent Fröhlich transformation, we have decoupled these lattices into two Aubry-André chains with two different λ_c that depend on the hopping t_d between sites of two chains with different energies and effective hopping parameters. Since the two effective chains are not coupled, their spectra may overlap such

that localized states (from one chain) and delocalized states (from the other chain) coexist at the same energy. Since the transitions happen in general at different values of λ for the two different chains, and the chain spectra are shifted relative to each other, one may encounter at the same energy a localized state from one chain, and a delocalized state from the other chain. It is relevant to note that this last models are link because in the ground state of the triangular lattice the critical quasi-disorder strength is equal to the critical quasi-disorder strength of an excited state of square lattice with shift, and viceversa.
In order to introduce Fröhlich's approach we modified the initial Hamiltonian adding a shift Δ into the energy for site of the first chain. We have determined this new parameter comparing the critical strength of the model introduced by *Sil et al.* in [23] and discussed by *Flach* and *Danieli* in [24] . The value of Δ turned to be equal to the vertical hopping between sites with equal energy.

In [24] it is suggested that a mobility edge in a quasi-1D network could be achieved choosing different energies for sites in the two chains. If we consider the model studied by *Sil et al.* with a chain shifted by one site and apply Fröhlich's approach we find again two decoupled Aubry-Andrè systems with two different nearest-neighbor hoppings, so no clear mobility edges appear.
A possible way to obtain, though the Frölich transformation, two decoupled chains with next nearest-neighbor hoppings is given by the introduction of a new hopping between the chains. In this way we could obtain localized and delocalized states separated by several mobility edges.

Appendix A

Some Commutators Calculations

Let's introduce four generic operators $\hat{A}$, $\hat{B}$, $\hat{C}$ and $\hat{D}$. The commutator and anticommutator between two operators are defined respectively as:

$$\left[\hat{A},\hat{B}\right] = \hat{A}\hat{B} - \hat{B}\hat{A}$$

$$\left\{\hat{A},\hat{B}\right\} = \hat{A}\hat{B} + \hat{B}\hat{A}$$

In a unify notation we can define a general commutator as:

$$\left[\hat{A},\hat{B}\right]_{\xi} = \hat{A}\hat{B} - \xi\hat{B}\hat{A} = -\xi\left[\hat{B},\hat{A}\right]_{\xi}$$

where $\xi = \pm 1$. For $\xi = 1$ the general commutator returns the boson commutator whereas for $\xi = -1$ returns the fermion anticommutator.
Now we have:

$$\begin{aligned}\left[\hat{A}\hat{B},\hat{C}\hat{D}\right] &= \hat{A}\hat{B}\hat{C}\hat{D} - \hat{C}\hat{D}\hat{A}\hat{B} = \hat{A}\hat{B}\hat{C}\hat{D} - \hat{C}\hat{A}\hat{B}\hat{D} + \hat{C}\hat{A}\hat{B}\hat{D} - \hat{C}\hat{D}\hat{A}\hat{B} \\ &= \left[\hat{A}\hat{B},\hat{C}\right]\hat{D} + \hat{C}\left[\hat{A}\hat{B},\hat{D}\right] \end{aligned} \tag{A.1}$$

We can explicit the commutator $\left[\hat{A}\hat{B},\hat{C}\right]$ in terms of the general commutator $[,]_{\xi}$, in fact:

$$\left[\hat{A}\hat{B},\hat{C}\right] = \hat{A}\hat{B}\hat{C} - \hat{C}\hat{A}\hat{B} = \hat{A}\hat{B}\hat{C} - \hat{A}\hat{C}\hat{B} + \hat{A}\hat{C}\hat{B} - \hat{C}\hat{A}\hat{B} = \hat{A}\left[\hat{B},\hat{C}\right] + \left[\hat{A},\hat{C}\right]\hat{B}$$

$$\left[\hat{A}\hat{B},\hat{C}\right] = \hat{A}\hat{B}\hat{C} - \hat{C}\hat{A}\hat{B} = \hat{A}\hat{B}\hat{C} + \hat{A}\hat{C}\hat{B} - \hat{A}\hat{C}\hat{B} - \hat{C}\hat{A}\hat{B} = \hat{A}\left\{\hat{B},\hat{C}\right\} - \left\{\hat{A},\hat{C}\right\}\hat{B}$$

So we obtain:

$$\left[\hat{A}\hat{B},\hat{C}\right] = \hat{A}\left[\hat{B},\hat{C}\right]_{\xi} + \xi\left[\hat{A},\hat{C}\right]_{\xi}\hat{B}$$

Finally we can write the commutator A.1 as

$$\left[\hat{A}\hat{B},\hat{C}\hat{D}\right] = \hat{A}\left[\hat{B},\hat{C}\right]_{\xi}\hat{D} + \xi\left[\hat{A},\hat{C}\right]_{\xi}\hat{B}\hat{D} + \hat{C}\hat{A}\left[\hat{B},\hat{D}\right]_{\xi} + \xi\hat{C}\left[\hat{A},\hat{D}\right]_{\xi}\hat{B}$$

Let's introduce single-particle operators $\hat{a}$ and $\hat{b}$ which satisfy the rules:

$$\begin{aligned}
\left[\hat{a}_n, \hat{b}_m\right]_\xi &= \left[\hat{a}_n, \hat{b}_m^\dagger\right]_\xi = 0 \\
\left[\hat{a}_n, \hat{a}_m\right]_\xi &= \left[\hat{a}_n^\dagger, \hat{a}_m^\dagger\right]_\xi = 0 \\
\left[\hat{b}_n, \hat{b}_m\right]_\xi &= \left[\hat{b}_n^\dagger, \hat{b}_m^\dagger\right]_\xi = 0 \\
\left[\hat{a}_n, \hat{a}_m^\dagger\right]_\xi &= \delta_{n,m} \\
\left[\hat{b}_n, \hat{b}_m^\dagger\right]_\xi &= \delta_{n,m}
\end{aligned}$$

Hence we can compute the following commutators independently of particle statistic.

$$\begin{aligned}
\left[\hat{a}_n^\dagger \hat{a}_n, \hat{a}_m^\dagger \hat{b}_m\right] &= \hat{a}_n^\dagger \left[\hat{a}_n, \hat{a}_m^\dagger\right]_\xi \hat{b}_m + \xi \left[\hat{a}_n^\dagger, \hat{a}_m^\dagger\right]_\xi \hat{a}_n \hat{b}_m + \hat{a}_m^\dagger \hat{a}_n^\dagger \left[\hat{a}_n, \hat{b}_m\right]_\xi + \xi \hat{a}_m^\dagger \left[\hat{a}_n^\dagger, \hat{b}_m\right]_\xi \hat{a}_n \\
&= \delta_{n,m} \hat{a}_n^\dagger \hat{b}_m
\end{aligned}$$

$$\begin{aligned}
\left[\hat{a}_n^\dagger \hat{a}_n, \hat{b}_m^\dagger \hat{a}_m\right] &= \hat{a}_n^\dagger \left[\hat{a}_n, \hat{b}_m^\dagger\right]_\xi \hat{a}_m + \xi \left[\hat{a}_n^\dagger, \hat{b}_m^\dagger\right]_\xi \hat{a}_n \hat{a}_m + \hat{b}_m^\dagger \hat{a}_n^\dagger \left[\hat{a}_n, \hat{b}_m\right]_\xi + \xi \hat{b}_m^\dagger \left[\hat{a}_n^\dagger, \hat{a}_m\right]_\xi \hat{a}_n \\
&= -\xi^2 \delta_{m,n} \hat{b}_m^\dagger \hat{a}_n = -\delta_{m,n} \hat{b}_m^\dagger \hat{a}_n
\end{aligned}$$

$$\begin{aligned}
\left[\hat{a}_n^\dagger \hat{b}_n, \hat{b}_m^\dagger \hat{a}_m\right] &= \hat{a}_n^\dagger \left[\hat{b}_n, \hat{b}_m^\dagger\right]_\xi \hat{a}_m + \xi \left[\hat{a}_n^\dagger, \hat{b}_m^\dagger\right]_\xi \hat{b}_n \hat{a}_m + \hat{b}_m^\dagger \hat{a}_n^\dagger \left[\hat{b}_n, \hat{a}_m\right]_\xi + \xi \hat{b}_m^\dagger \left[\hat{a}_n^\dagger, \hat{a}_m\right]_\xi \hat{b}_n \\
&= \delta_{n,m} \hat{a}_n^\dagger \hat{a}_m - \xi^2 \delta_{n,m} \hat{b}_m^\dagger \hat{b}_n = \delta_{n,m} \hat{a}_n^\dagger \hat{a}_m - \delta_{n,m} \hat{b}_m^\dagger \hat{b}_n
\end{aligned}$$

$$\begin{aligned}
\left[\hat{a}_n^\dagger \hat{b}_n, \hat{a}_m^\dagger \hat{b}_m\right] &= \hat{a}_n^\dagger \left[\hat{b}_n, \hat{a}_m^\dagger\right]_\xi \hat{b}_m + \xi \left[\hat{a}_n^\dagger, \hat{a}_m^\dagger\right]_\xi \hat{b}_n \hat{b}_m + \hat{a}_m^\dagger \hat{a}_n^\dagger \left[\hat{b}_n, \hat{b}_m\right]_\xi + \xi \hat{a}_m^\dagger \left[\hat{a}_n^\dagger, \hat{b}_m\right]_\xi \hat{b}_n \\
&= 0
\end{aligned}$$

Appendix B

A series Calculation

Lemma B.0.1. For $s = 0, 1$ we have the following identity:

$$\sum_r e^{-(p+is\pi)|r|} e^{imr2\pi q} = \frac{\sinh(p)}{\cosh(p) - \cos(m2\pi q)e^{is\pi}}$$

Proof.

$$\begin{aligned}
\sum_r e^{-(p+is\pi)|r|} e^{imr2\pi q} &= \sum_{r=-\infty}^{-1} e^{(p+is\pi)r} e^{imr2\pi q} + \sum_{r=1}^{\infty} e^{-(p+is\pi)r} e^{imr2\pi q} + 1 \\
&= \sum_{r=0}^{\infty} e^{-(p+is\pi)r} \left(e^{-imr2\pi q} + e^{imr2\pi q} \right) - 1 \\
&= 2\sum_{r=0}^{\infty} e^{-(p+is\pi)r} \cos(mr2\pi q) - 1
\end{aligned}$$

In this proof we consider only the case $s = 0$. Now we calculate explicitly the following series:

$$\sum_{r=0}^{\infty} e^{(-p)r} e^{ixr}$$

$$\begin{aligned}
\sum_{r=0}^{\infty} \left(e^{(-p)} e^{ix} \right)^r &= \frac{1}{1 - e^{(-p)} e^{ix}} \\
&= \frac{e^p}{e^p - e^{ix}} = \frac{e^p}{e^p - \cos(x) - i\sin(x)} \\
&= \frac{e^p}{e^p - \cos(x) - i\sin(x)} \frac{e^p - \cos(x) + i\sin(x)}{e^p - \cos(x) + i\sin(x)} \\
&= \frac{e^{2p} - e^p \cos(x)}{(e^p - \cos(x))^2 + \sin^2(x)} + i \frac{\sin(x)}{(e^p - \cos(x))^2 + \sin^2(x)} \\
&= \frac{e^{2p} - e^p \cos(x)}{e^{2p} - 2e^p \cos(x) + \cos(x)^2 + \sin(x)^2} + i \frac{\sin(x)}{e^{2p} - 2e^p \cos(x) + \cos(x)^2 + \sin(x)^2} \\
&= \frac{e^p - \cos(x)}{2\cosh(p) - 2\cos(x)} + i \frac{\sin(x) e^{-p}}{2\cosh(p) - 2\cos(x)}
\end{aligned}$$

and have taken in consideration the real part:

$$\sum_{r=0}^{\infty} e^{(-p)r}\cos(xr) = \mathfrak{R}e\left(\sum_{r=0}^{\infty} e^{(-p)r}e^{ixr}\right) = \frac{e^p - \cos(x)}{2\cosh(p) - 2\cos(x)}$$

Finally in the our case we get:

$$\sum_{r} e^{-p|r|}e^{imr2\pi q} = 2\frac{e^p - \cos(m2\pi q)}{2\cosh(p) - 2\cos(m2\pi q)} - 1 = \frac{\sinh(p)}{\cosh(p) - \cos(m2\pi q)}$$

□

Appendix C

A canonical transformation

Let us have an Hamiltonian

$$\mathcal{H} = \mathcal{H}_0 + \mathcal{H}_1$$

We can perform a canonical trasformation to derive an effective Hamiltonian by eliminating degrees of freedom with low energy excitations. One of the most well-known applications is Fröhlich's transformation that was applied to derive an attractive electron-electron interaction from the original electron-phonon interaction.
Fröhlich's approach consists into perform a unitary transformation $\tilde{\mathcal{H}} = e^{-g\hat{S}}\mathcal{H}e^{g\hat{S}}$, defined by an anti-Hermitian operator $\hat{S}$ [25], to the Hamiltonian $\mathcal{H}$. Here g is an arbitrary parameter, introduced to stress weak interaction between chains and can be set to 1 during and after the calculations.
Now we evaluate the transformation order by order:

$$\begin{aligned}
\tilde{\mathcal{H}} = e^{-g\hat{S}}\mathcal{H}e^{g\hat{S}} &= \left(1 - g\hat{S} + g^2\frac{\hat{S}^2}{2} + O(g^3)\right)(\mathcal{H}_0 + g\mathcal{H}_1)\left(1 + g\hat{S} + g^2\frac{\hat{S}^2}{2} + O(g^3)\right) \\
&= \left(1 - g\hat{S} + g^2\frac{\hat{S}^2}{2} + O(g^3)\right)\left(\mathcal{H}_0 + g\mathcal{H}_0\hat{S} + g^2\mathcal{H}_0\frac{\hat{S}\hat{S}}{2} + g\mathcal{H}_1 + g^2\mathcal{H}_1\hat{S} + O(g^3)\right) \\
&= \mathcal{H}_0 + g\mathcal{H}_0\hat{S} + g^2\mathcal{H}_0\frac{\hat{S}\hat{S}}{2} + g\mathcal{H}_1\hat{S} - g\hat{S}\mathcal{H}_0 - g^2\hat{S}\mathcal{H}_0\hat{S} - g^2\hat{S}\mathcal{H}_0\hat{S} - g^2\hat{S}\mathcal{H}_1 + g^2\frac{\hat{S}\hat{S}}{2}\mathcal{H}_0 + O(g^3) \\
&= \mathcal{H}_0 + g\left(\mathcal{H}_1 + \left[\mathcal{H}_0, \hat{S}\right]\right) + g^2\left(\left[\mathcal{H}_1, \hat{S}\right] + \mathcal{H}_0\frac{\hat{S}\hat{S}}{2} - \frac{\hat{S}\mathcal{H}_0\hat{S}}{2} - \frac{\hat{S}\mathcal{H}_0\hat{S}}{2} + \frac{\hat{S}\hat{S}\mathcal{H}_0}{2}\right) + O(g^3)
\end{aligned}$$

From the fact that:

$$\mathcal{H}_0\frac{\hat{S}\hat{S}}{2} - \frac{\hat{S}\mathcal{H}_0\hat{S}}{2} - \frac{\hat{S}\mathcal{H}_0\hat{S}}{2} + \frac{\hat{S}\hat{S}\mathcal{H}_0}{2} = \frac{1}{2}\left[\left[\mathcal{H}_0, \hat{S}\right], \hat{S}\right]$$

we obtain:

$$\tilde{\mathcal{H}} = \mathcal{H}_0 + g\left(\mathcal{H}_1 + \left[\mathcal{H}_0, \hat{S}\right]\right) + g^2\left(\left[\mathcal{H}_1 + \frac{1}{2}\left[\mathcal{H}_0, \hat{S}\right], S\right]\right) + O(g^3)$$

Frolich eliminated the linear term in g by requiring:

$$\mathcal{H}_1 + \left[\mathcal{H}_0, \hat{S}\right] = 0 \tag{C.1}$$

to get the generator $\hat{S}$. With this constraint the new Hamiltonian is:

$$\tilde{\mathcal{H}} = \mathcal{H}_0 + \frac{1}{2}\left[\mathcal{H}_1, S\right]$$

Bibliography

[1] Diederik S Wiersma, Paolo Bartolini, Ad Lagendijk, and Roberto Righini. Localization of light in a disordered medium. *Nature*, 390(6661):671, 1997.

[2] Tal Schwartz, Guy Bartal, Shmuel Fishman, and Mordechai Segev. Transport and anderson localization in disordered two-dimensional photonic lattices. *Nature*, 446(7131):52, 2007.

[3] Martin Störzer, Peter Gross, Christof M. Aegerter, and Georg Maret. Observation of the critical regime near anderson localization of light. *Phys. rev. lett.*, 96:063904, 6, 2006. DOI: 10.1103/PhysRevLett.96.063904. URL: https://link.aps.org/doi/10.1103/PhysRevLett.96.063904.

[4] Hefei Hu, A. Strybulevych, J. H. Page, S. E. Skipetrov, and B. A. van Tiggelen. Localization of ultrasound in a three-dimensional elastic network. *Nat phys*, 4:945, 2008. URL: http://dx.doi.org/10.1038/nphys1101.

[5] Sanli Faez, Anatoliy Strybulevych, John H. Page, Ad Lagendijk, and Bart A. van Tiggelen. Observation of multifractality in anderson localization of ultrasound. *Phys. rev. lett.*, 103:155703, 15, 2009. DOI: 10.1103/PhysRevLett.103.155703. URL: https://link.aps.org/doi/10.1103/PhysRevLett.103.155703.

[6] Juliette Billy, Vincent Josse, Zhanchun Zuo, Alain Bernard, Ben Hambrecht, Pierre Lugan, David Clement, Laurent Sanchez-Palencia, Philippe Bouyer, and Alain Aspect. Direct observation of anderson localization of matter waves in a controlled disorder. *Nature*, 453:891, 2008. URL: http://dx.doi.org/10.1038/nature07000.

[7] Giacomo Roati, Chiara D/'Errico, Leonardo Fallani, Marco Fattori, Chiara Fort, Matteo Zaccanti, Giovanni Modugno, Michele Modugno, and Massimo Inguscio. Anderson localization of a non-interacting bose-einstein condensate. *Nature*, 453:895, 2008. URL: http://dx.doi.org/10.1038/nature07071.

[8] Laurent Sanchez-Palencia and Maciej Lewenstein. Disordered quantum gases under control. *Nat phys*, 6:87, 2010. URL: http://dx.doi.org/10.1038/nphys1507.

[9] Cheng Chin, Rudolf Grimm, Paul Julienne, and Eite Tiesinga. Feshbach resonances in ultracold gases. *Rev. mod. phys.*, 82:1225–1286, 2, 2010. DOI: 10.1103/RevModPhys.82.1225. URL: https://link.aps.org/doi/10.1103/RevModPhys.82.1225.

[10] Serge Aubry and Gilles André. Analyticity breaking and anderson localization in incommensurate lattices. *Ann. israel phys. soc*, 3(133):18, 1980. URL: https://www.researchgate.net/publication/265502988_Analyticity_breaking_and_Anderson_localization_in_incommensurate_lattices.

[11] Christian Aulbach, André Wobst, Gert-Ludwig Ingold, Peter Hänggi, and Imre Varga. Phase-space visualization of a metal–insulator transition. *New journal of physics*, 6(1):70, 2004.

[12] Svetlana Ya Jitomirskaya. Metal-insulator transition for the almost mathieu operator. *Annals of mathematics*, 150(3):1159–1175, 1999.

[13] Philip George Harper. Single band motion of conduction electrons in a uniform magnetic field. *Proceedings of the physical society. section a*, 68(10):874, 1955.

[14] Rudolph Peierls. Zur theorie des diamagnetismus von leitungselektronen. *Zeitschrift für physik a hadrons and nuclei*, 80(11):763–791, 1933.

[15] Douglas R. Hofstadter. Energy levels and wave functions of bloch electrons in rational and irrational magnetic fields. *Phys. rev. b*, 14:2239–2249, 6, 1976. DOI: 10.1103/PhysRevB.14.2239. URL: https://link.aps.org/doi/10.1103/PhysRevB.14.2239.

[16] Mahito Kohmoto. Metal-insulator transition and scaling for incommensurate systems. *Phys. rev. lett.*, 51:1198–1201, 13, 1983. DOI: 10.1103/PhysRevLett.51.1198. URL: https://link.aps.org/doi/10.1103/PhysRevLett.51.1198.

[17] D. J. Thouless. Bandwidths for a quasiperiodic tight-binding model. *Phys. rev. b*, 28:4272–4276, 8, 1983. DOI: 10.1103/PhysRevB.28.4272. URL: https://link.aps.org/doi/10.1103/PhysRevB.28.4272.

[18] R. Ramakumar, A.N. Das, and S. Sil. Lattice bosons in a quasi-disordered environment: the effects of next-nearest-neighbor hopping on localization and bose–einstein condensation. *Physica a: statistical mechanics and its applications*, 401:214 –223, 2014. ISSN: 0378-4371. DOI: https://doi.org/10.1016/j.physa.2014.01.049. URL: http://www.sciencedirect.com/science/article/pii/S0378437114000612.

[19] Yi Zhang, Daniel Bulmash, Akash V Maharaj, Chao-Ming Jian, and Steven A Kivelson. The almost mobility edge in the almost mathieu equation. *Arxiv preprint arxiv:1504.05205*, 2015.

[20] A. D. Zdetsis, C. M. Soukoulis, and E. N. Economou. Fractal character of wave functions in one-dimensional incommensurate systems. *Phys. rev. b*, 33:4936–4940, 7, 1986. DOI: 10.1103/PhysRevB.33.4936. URL: https://link.aps.org/doi/10.1103/PhysRevB.33.4936.

[21] C. M. Soukoulis and E. N. Economou. Fractal character of eigenstates in disordered systems. *Phys. rev. lett.*, 52:565–568, 7, 1984. DOI: 10.1103/PhysRevLett.52.565. URL: https://link.aps.org/doi/10.1103/PhysRevLett.52.565.

[22] J. Biddle and S. Das Sarma. Predicted mobility edges in one-dimensional incommensurate optical lattices: an exactly solvable model of anderson localization. *Phys. rev. lett.*, 104:070601, 7, 2010. DOI: 10.1103/PhysRevLett.104.070601. URL: https://link.aps.org/doi/10.1103/PhysRevLett.104.070601.

[23] Shreekantha Sil, Santanu K. Maiti, and Arunava Chakrabarti. Metal-insulator transition in an aperiodic ladder network: an exact result. *Phys. rev. lett.*, 101:076803, 7, 2008. DOI: 10.1103/PhysRevLett.101.076803. URL: https://link.aps.org/doi/10.1103/PhysRevLett.101.076803.

[24] Sergej Flach and Carlo Danieli. Comment on" metal-insulator transition in an aperiodic ladder network: an exact result". *Arxiv preprint arxiv:1402.2742*, 2014.

[25] Przemysław Tarasewicz and Dominik Baran. Extension of the fröhlich method to 4-fermion interactions. *Phys. rev. b*, 73:094524, 9, 2006. DOI: 10.1103/PhysRevB.73.094524. URL: https://link.aps.org/doi/10.1103/PhysRevB.73.094524.